Role of gut and skin microbiota and spleen in mice model of psoriasis

（乾癬モデルマウスにおける腸・皮膚の細菌叢と脾臓の役割）

千葉大学大学院医学薬学府

先端医学薬学専攻

（主任：橋本 謙二 教授）

新野（橋本）啓代

Background

Psoriasis is a common and chronic inflammatory disorder that presents with scaly plaques on the skin. Patients with psoriasis have higher incidences of systemic complications, including psoriatic arthritis, cardiovascular disease, metabolic syndrome, inflammatory bowel disease, and depression. Although the detailed molecular mechanisms of psoriasis are unclear, excessive immunological abnormalities play a role in pathogenesis of psoriasis. Several reports suggested that psoriasis and the above-mentioned comorbidities might be associated with gut microbiota. Imiquimod (IMQ), a Toll-like receptor 7 agonist, has been widely used as animal model of psoriasis. Spleen has important functions in immunity, and splenomegaly is observed in IMQ-treated mice.

The PhD thesis is consisted of two parts. The part one is abnormal composition of microbiota in the gut and skin of IMQ-treated mice. The part two is the effects of splenectomy on skin inflammation and psoriasis-like phenotype of IMQ-treated mice.

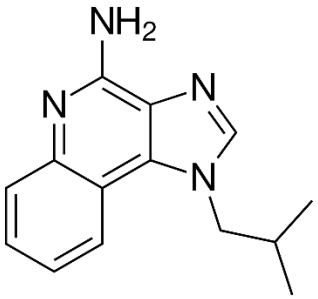

Chemical structure of imiquimod (IMQ)

Part-1

Abnormal composition of microbiota in the gut and skin of imiquimod-treated mice

Abstract

Psoriasis is a chronic, inflammatory skin disease. Although the precise etiology of psoriasis remains unclear, gut–microbiota axis might play a role in the pathogenesis of the disease. Here we investigated whether the composition of microbiota in the intestine and skin is altered in the imiquimod (IMQ)-treated mouse model of psoriasis. Topical application of IMQ to back skin caused significant changes in the composition of microbiota in the intestine and skin of IMQ-treated mice compared to control mice. The LEfSe algorithm identified the species *Staphylococcus lentus* as potential skin microbial marker for IMQ group. Furthermore, there were correlations for several microbes between the intestine and skin, suggesting a role of skin–gut–microbiota in IMQ-treated mice. Levels of succinic acid and lactic acid in feces from IMQ-treated mice were significantly higher than control mice. Moreover, the predictive functional analysis of the microbiota in the intestine and skin showed that IMQ caused alterations in several KEGG pathways. In conclusion, the current data indicated that topical application with IMQ to skin alters the composition of the microbiota in the gut and skin of host. It is likely that skin–gut microbiota axis plays a role in pathogenesis of psoriasis.

Keywords: Imiquimod; Intestine; Microbiota; Psoriasis; Succinic acid; Skin

Introduction

Psoriasis is a common chronic inflammatory disease of skin. A recent systematic review reports that the prevalence of psoriasis in children and adults ranged from 0% to 1.37% and 0.51% to 11.43%, respectively (1). Furthermore, psoriasis is associated strongly with depression, cardiovascular disease, diabetes, and metabolic syndrome, which influence quality of life in patients (2-6). Although excessive activation of the immune system plays a major role in the pathogenesis of psoriasis, the precise pathogenesis of this disease remains unclear (3,6).

Accumulating evidence suggests the physiological and metabolic roles of the microbiota in human health and diseases (7-13). It is well known that microbes are colonized in the gastrointestinal tract, skin, oral mucosa, vagina and airway in the human, and that the colon is the most abundant site for microbes, followed by the skin (14). Altered composition of gut microbiota in patients with psoriasis has been reported (15-19). Furthermore, there are also several reports showing abnormal composition of skin microbiota in patients with psoriasis (20-25). These findings suggest that alterations in the microbiome in the intestine and on the skin might play a role in the pathogenesis of psoriasis, and that improvement of altered composition of microbiota could be a therapeutic approach for this disease (14).

Imiquimod (IMQ), a Toll-like receptor 7 agonist, has been used widely as mouse model of psoriasis to understand the inflammatory responses of the skin (26,27). It is also reported that depletion of microbiota by antibiotics ameliorated IMQ-treated psoriasis in mice, suggesting the role of microbiota in IMQ-induced skin inflammation (22,28). Furthermore, treatment with IMQ caused altered composition of gut microbiota in mice (29). Moreover, mice treated with antibiotics showed higher abundance of the genus *Lactobacillus* in the intestine and on the skin (30). Interestingly, it is recognized that the skin neuroendocrine system acts by preserving and maintaining the skin structural and functional integrity (31), and that the skin is a sensory organ endowed with neuroendocrine activities (32). However, as far as we know, there are no reports showing altered composition of microbes in the intestine and on the skin of IMQ-treated mice.

The present study was undertaken to examine whether topical application of IMQ to skin could influence the composition of microbiota in the intestine and on the skin of adult mice. Using 16S rRNA sequencing, we analyzed the composition of microbiota in the intestine and on the skin of control and IMQ-treated mice. It is well known that short chain fatty acids (SCFAs), the main metabolites produced by microbiota in the gastrointestinal tract, play an important role in the metabolic functions in human and rodents (33-36). Therefore, we measured levels of SCFAs (i.e., acetic acid, propionic acid, butyric acid, lactic acid, and succinic acid) in the fecal samples.

Results

Effects of IMQ on the psoriasis-like score, body weight changes, spleen weight, and pathology of back skin

IMQ-treated mice developed psoriasis-like dermatitis compared to control mice (**Figure 1a**). Cumulative score of IMQ-treated mice was significantly higher than that of control mice (**Figure 1b**). Furthermore, the body weight in the IMQ-treated mice was significantly lower than that of control mice (**Figure 1c**). Moreover, the weight of spleen in the IMQ-treated mice was significantly higher than that of control mice (**Figure 1d**), consistent with previous reports (27,37-39). Representative H&E staining in the back skin showed parakeratosis with microabscess, acanthosis and an inflammatory infiltrate of the upper dermis in the IMQ-treated mice (**Figure 1e**).

Composition of gut microbiota

Using alpha- and beta-diversity, we examined the composition of the gut microbiota in fecal samples. Mann-Whitney U-test showed a significant difference in the observed OTUs (**Figure 2a**). In contrast, there were no changes for ACE and Shannon indices between the two groups (**Figures 2b and 2c**). Beta diversity based on analysis of similarities (ANOSIM) was used to measure the degree of difference in bacterial community, including principal component analysis (PCA) of the OTU composition and principal coordinate analysis (PCoA) of weighted UniFrac distances. PCA demonstrated a significant difference in the microbiome (ANOSIM, $R = 0.6294$, $P = 0.001$) (**Figure 2d**). In addition, PCoA of weighted UniFrac distances indicated a clear separation of IMQ group from control group (ANOSIM, $R = 0.3236$, $P = 0.002$) (**Figure 2e**).

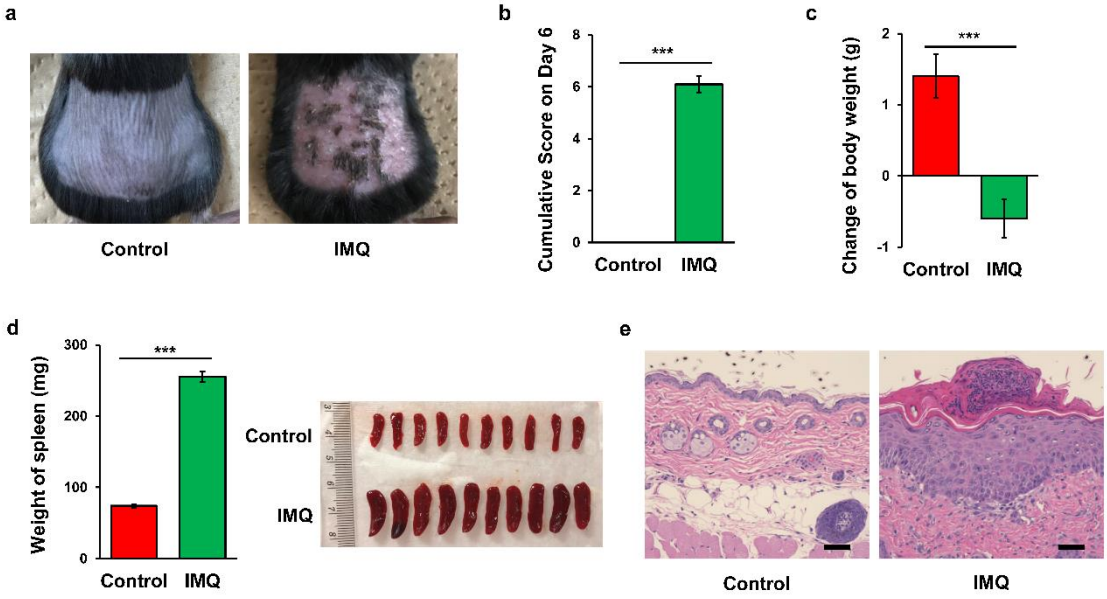

Figure 1. IMQ-induced psoriasis-like model

(a): Mice were treated topically with 5% IMQ cream or control cream on the shaved backs for five consecutive days. The representative photos of back skin from the two groups. (b): Cumulative score on day 6 of two groups ($P < 0.001$). (c): Change of body weight for the two groups ($P < 0.001$). (d): Weight of spleen ($P < 0.001$). The photos of spleen from the control and IMQ group. (e): HE staining of the back skin of the two groups. Scale bar = 50 μm. The values represent the mean ± S.E.M. (n = 10). ***$P < 0.001$.

The changes of the abundant taxa were analyzed by the LEfSe algorithm. The color differences illustrated differences in the abundant taxa between the two groups. LEfSe analysis showed that IMQ group produced significantly different effects on gut microbiota (**Figure 2f**). Five mixed-level phylotypes, including the species *Lactobacillus intestinalis*, *Lactobacillus reuteri*, *Bacteroides uniformis*, the genus *Bacteroides*, and the family *Bacteroidaceae*, were identified as potential gut microbial markers for the IMQ group (**Figure 2g**).

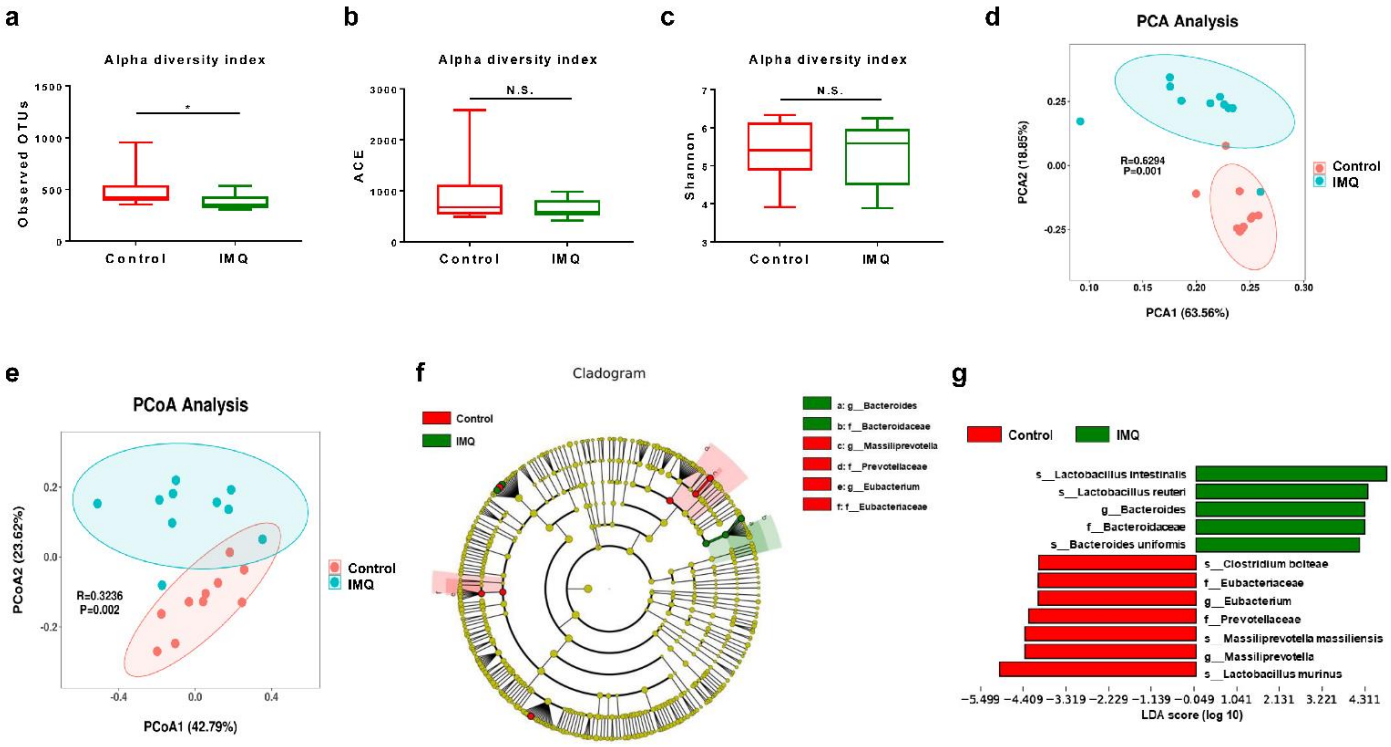

Figure 2. Effects of IMQ on the composition of gut microbiota in alpha-diversity and beta-diversity

(a): Alpha-diversity index of observed OTUs (Mann-Whitney U test, U = 21, P = 0.029). (b): Alpha-diversity index of ACE (Mann-Whitney U test, U = 21, P = 0.353). (c): Alpha-diversity index of Shannon (Mann-Whitney U test, U = 45, P = 0.739). (d): PCA of beta-diversity based on the OTU level (ANOSIM, R = 0.6294, P = 0.001). Each point represents a single sample which is color-coded according to group, and the two principal components (PC1 and PC2) explained 63.56% and 18.85%. (e): PCoA plot using weighted UniFrac distance (ANOSIM, R = 0.3236, P = 0.002). Each point represents a single sample and the two principal components (PCoA1 and PCoA2) explained 42.79% and 23.62%. (f): LEfSe cladogram (LDA score > 4.0, P < 0.05) indicated differentially abundant taxa between control group and IMQ group. Each circle represents the taxonomic categories from the species level as the outermost circle to phylum level as the innermost cycle. (g): Histograms revealed differentially abundant taxa with LDA score (log10) > 4.0 and P < 0.05 between the control group and IMQ group. The LDA scores of the control group was negative, while those of the IMQ group was positive. The values represent the mean ± S.E.M. (n = 10). *P < 0.05. NS: not significant.

Composition of the gut microbiota at the taxonomic level

At the phylum, there were no changes between the two groups (**Figure S1**). At the genus level, the abundance of *Bacteroides*, *Parabacteroides*, *Staphylococcus, Faecalimonas*, and *Alistipes* was significantly different between the two groups (**Figure S2 and Table S1**). At the species level, the abundance of *Lactobacillus murinus, Lactobacillus intestinalis, Lactobacillus reuteri, Lactobacillus taiwanensis, Bacteroides uniformis, Bacteroides acidifaciens, Bacteroides sartorii, Staphylococcus lentus, and Parabacteroides distasonis* was significantly different between the two groups (**Figure S3 and Table S2**).

Composition of skin microbiota

The composition of the microbiota on the back skin was analyzed. Mann-Whitney U-test showed significant differences in the observed OTUs, ACE, and Shannon (**Figures 3a-3c**). Beta-diversity analysis using PCA demonstrated significant differences between IMQ group and control group (ANOSIM, R = 1.000, P = 0.001) (**Figure 3d**). Furthermore, significant separation was observed between the two groups on PCoA of weighted UniFrac distances (ANOSIM, R = 0.7293, P = 0.001) (**Figure 3e**).

LEfSe difference analysis showed that IMQ group produced significantly different effects on skin microbiota (**Figure 3f**). Six mixed-level phylotypes, including the species *Staphylococcus lentus*, the genus *Staphylococcus*, the family *Staphylcoccaceae*, the order *Bacillales*, the class *Bacilli*, and the phylum *Firmicutes* were identified as potential skin microbial markers for the IMQ group (**Figure 3g**).

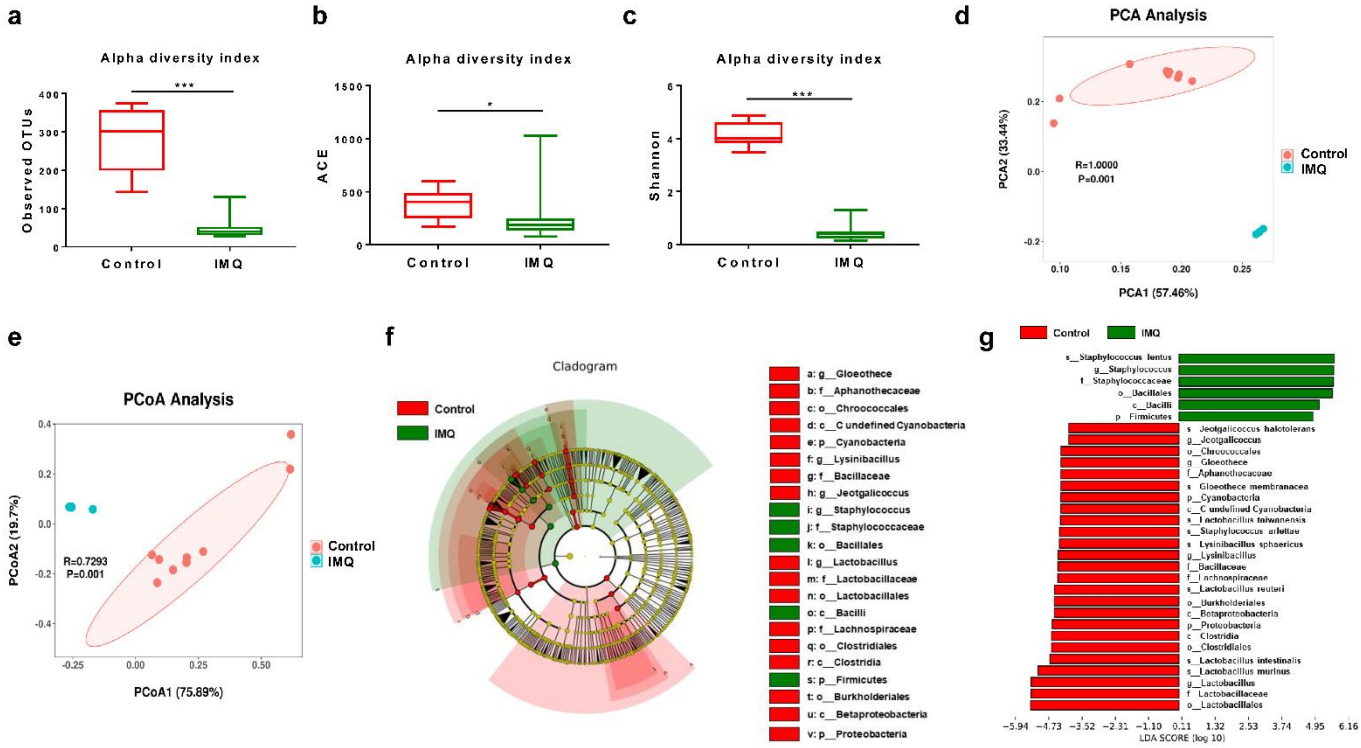

Figure 3. Effects of IMQ on the composition of skin microbiota in alpha-diversity and beta-diversity

(a): Alpha-diversity index of observed OTUs (Mann-Whitney U test, U = 0, P = 0.000). (b): Alpha-diversity index of ACE (Mann-Whitney U test, U = 20, P = 0.023). (c): Alpha-diversity index of Shannon (Mann-Whitney U test, U = 0, P = 0.000). (d): PCA of beta-diversity based on the OTU level (ANOSIM, R = 1.000, P = 0.001). Each point represents a single sample color-coded according to group, and the two principal components (PC1 and PC2) explained 57.46% and 33.44%. (e): PCoA plot using upon weighted UniFrac distance (ANOSIM, R = 0.7293, P = 0.001). Each point represents a single sample and the two principal components (PCoA1 and PCoA2) explained 75.89% and 19.7%. (f): LEfSe cladogram (LDA score > 4.0, P < 0.05) indicated differentially abundant taxa between control group and IMQ group. Each circle represents the taxonomic categories from the species level as the outermost circle to phylum level as the innermost cycle. (g): Histograms revealed differentially abundant taxa with LDA score (log10) > 4.0 and P < 0.05 between the control group and IMQ group. The LDA scores of the control group was negative, while those of the IMQ group was positive. The values represent the mean ± S.E.M. (n = 10). *P < 0.05; ***P < 0.001.

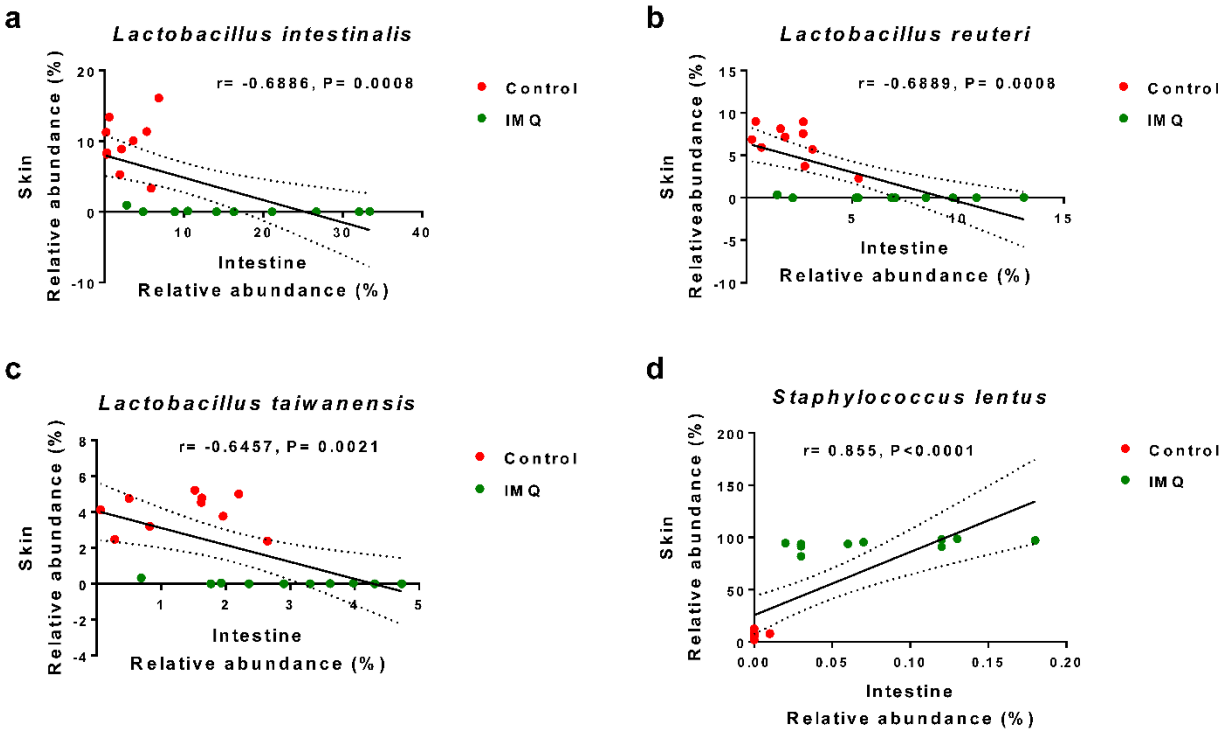

Figure 4. The correlations between bacterial relative abundance in the intestine and skin

(a): There was a significant negative correlation (r = −0.6886, P = 0.0008) of the relative abundance of the species *Lactobacillus intestinalis* between the intestine and the skin. (b): There was a significant negative correlation (r = −0.6889, P = 0.0008) of the relative abundance of the species *Lactobacillus reuteri* between the intestine and the skin. (c): There was a significant negative correlation (r = −0.6457, P = 0.0021) of the relative abundance of the species *Lactobacillus taiwanensis* between the intestine and the skin. (d): There was a significant positive correlation (r = 0.855, P < 0.0001) of the relative abundance of the species *Staphylococcus lentus* between the intestine and the skin. The values represent the mean ± S.E.M. (n = 10).

Composition of the skin microbiota at the taxonomic level

At the phylum level, the abundance of *Firmicutes, Proteobacteria, Cyanobacteria, Actinobacteria,* and *Bacteroidetes* was significantly different between the two groups (**Figure S4 and Table S3**). At the genus level, the most abundant bacteria on the skin of IMQ-treated mice was *Staphylococcus* (the mean = 98.5%) whereas the level of *Staphylococcus* on the skin of control mice was low (the mean = 16.2%) (**Figure S5**). Furthermore, the abundance of sixteen bacteria were significantly different between the two groups (**Figure S5 and Table S4**). At the species level, the most abundant bacteria

on the skin of IMQ-treated mice was *Staphylococcus lentus* (the mean is 93.5%) whereas the level of *Staphylococcus lentus* on the skin of control mice was very low (the mean is 7.14%) (**Figure S6**). Furthermore, the abundance of fourteen bacteria were significantly different between the two groups (**Figure S6 and Table S5**).

Correlations between the skin microbiota and the gut microbiota

At the species level, we found several microbes which were significantly altered in the intestine and on the skin between the two groups (**Tables S2 and S5**). Interestingly, there were negative correlations for *Lactobacillus intestinalis*, *Lactobacillus reuteri*, and *Lactobacillus taiwanensis* between the intestine and the skin (**Figures 4a-4c**). In contrast, there was a positive correlation for *Staphylococcus lentus* between the intestine and the skin (**Figure 4d**).

SCFAs in fecal samples and their correlations with the relative bacterial abundance

The levels of succinic acid and lactic acid in the IMQ group were significantly higher than the control groups (**Table 1**). In contrast, there were no changes for acetic acid, propionic acid, and n-butyric acid between the two groups (**Table 1**).

Next, we examined the possible correlations between the relative abundance of microbes and SCFA levels in fecal samples. The succinic acid was significantly correlated with the relative abundance of the genus *Parabacteroides* ($r = -0.464$, $P = 0.0393$) (**Figure 5a**), the genus *Staphylococcus* ($r = 0.4981$, $P = 0.0254$) (**Figure 5b**), the species *Parabacteroides distasonis* ($r = -0.485$, $P = 0.0302$) (**Figure 5c**), the species *Staphylococcus lentus* ($r = 0.4807$, $P = 0.0319$) (**Figure 5d**) and the species *Lactobacillus intestinalis* ($r = 0.4492$, $P = 0.0469$) (**Figure 5e**) in the two groups. A significant negative correlation between the relative abundance of the genus *Parabacteroides* ($r = -0.5079$, $P = 0.0222$) and lactic acid was observed in two groups (**Figure 5f**).

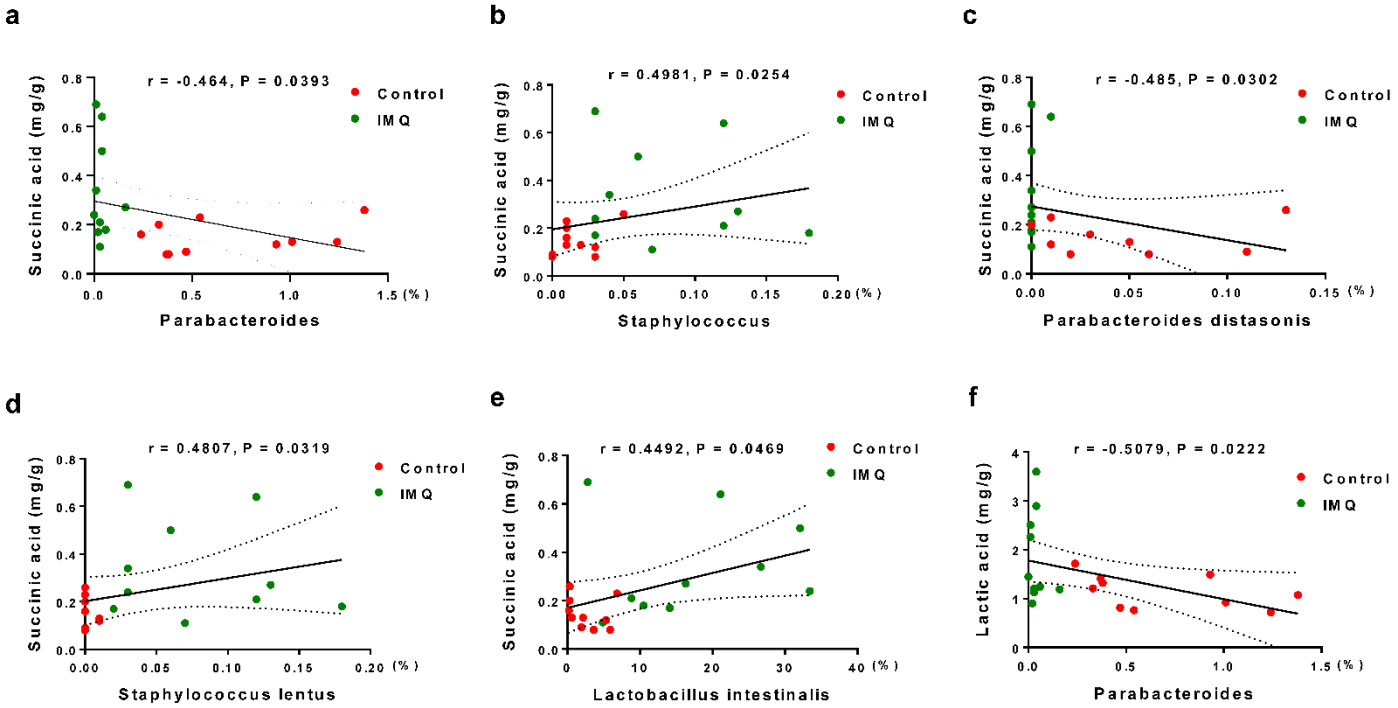

Figure 5. The correlations between bacterial relative abundance and SCFAs

(a): A significant negative correlation (r = −0.464, P = 0.0393) between the relative abundance of the genus *Parabacteroides* and succinic acid was shown in the control group and IMQ group. (b): A significant positive correlation (r = 0.4981, P = 0.0254) between the relative abundance of the genus *Staphylococcus* and succinic acid was shown in the two groups. (c): A significant negative correlation (r = −0.485, P = 0.0302) between the relative abundance of the species *Parabacteroides distasonis* and succinic acid was shown in the two groups. (d): A significant positive correlation (r = 0.4807, P = 0.0319) between the relative abundance of the species *Staphylococcus lentus* and succinic acid in the two groups. (e): A significant positive correlation (r = 0.4492, P = 0.0469) between the relative abundance of the species *Lactobacillus intestinalis* and succinic acid in the two groups. (f): There was a significant negative correlation (r = −0.5079, P = 0.0222) between the relative abundance of the genus *Parabacteroides* and lactic acid in the two groups. The values represent the mean ± S.E.M. (n = 10).

Predictive functional metagenomes

In gut microbiota, two pathways on KEGG level 2, including cardiovascular disease, and endocrine and metabolic disease were significantly different between the two groups (**Figure 6**). In skin microbiota, four pathways on KEGG level 3, including

sphingolipid signaling pathway, coronavirus disease (COVID-19), steroid degradation, and renin secretion were significantly different between the two groups (**Figure 7**).

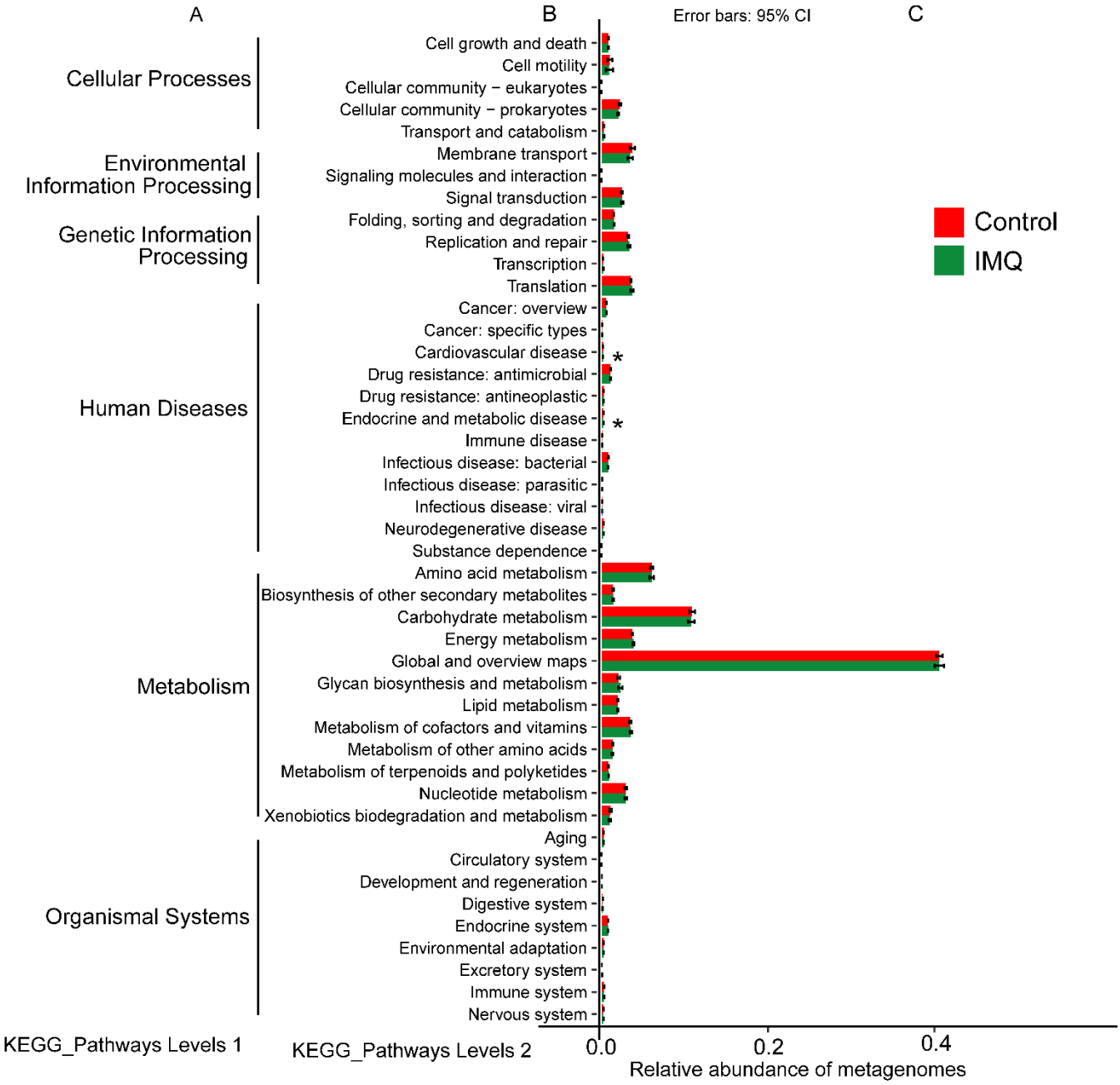

Figure 6. Relative abundance of KEGG pathways of functional categories in the gut microbiota

Functional predictions of the gut microbiota between the control group and IMQ group. Significant differences of KEGG pathways at level 2 were detected using STAMP software based on the KEGG pathway database (www.kegg.jp/kegg1.html). $^{*}P < 0.05$.

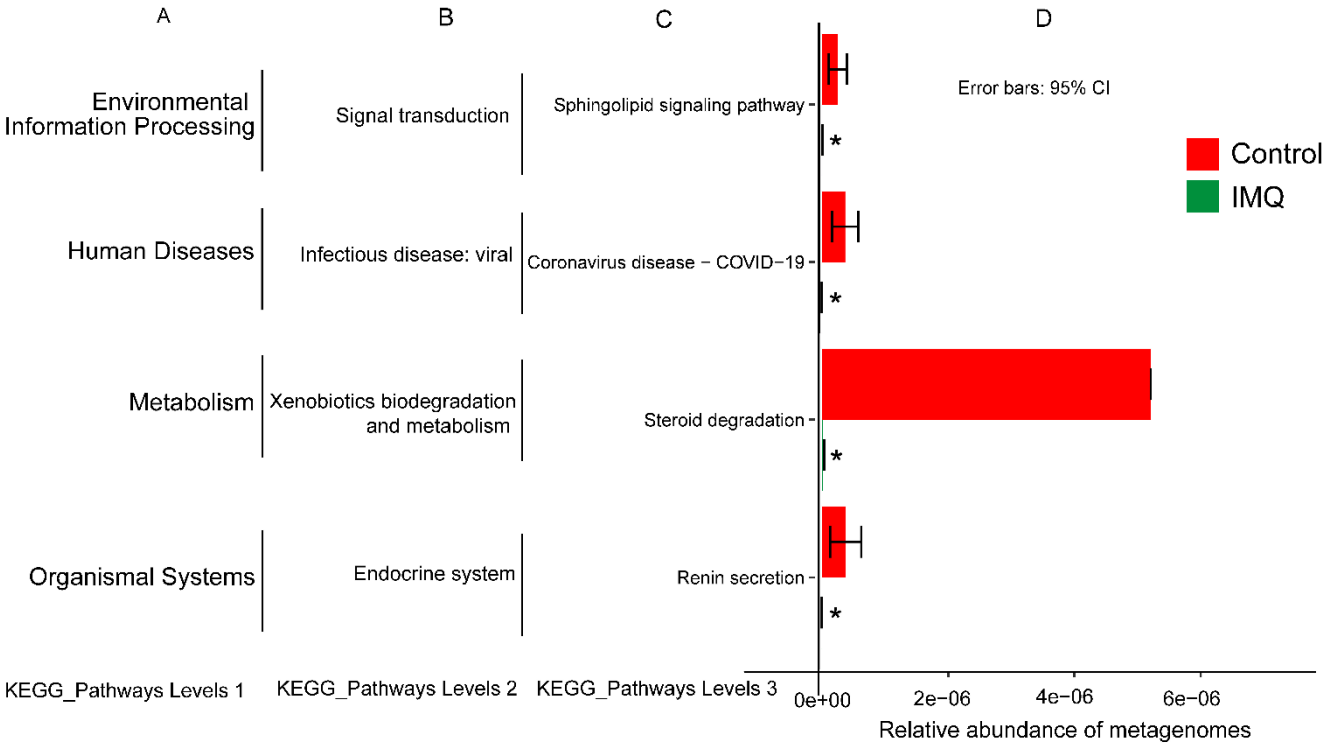

Figure 7. Relative abundance of KEGG pathways of functional categories in the skin microbiota

Functional predictions of the skin microbiota between the control group and IMQ group. Significant differences of KEGG pathways at level 3 were detected using STAMP software based on the KEGG pathway database (www.kegg.jp/kegg1.html). $^{*}P < 0.05$.

Table 1. Levels of short-chain fatty acids (SCFAs) in the fecal samples.

SCFAs (mg/g)	Control	IMQ	Student's t-test
Succinic acid	**0.146 ± 0.020**	**0.335 ± 0.065**	**df= 18, t= -2.767, P= 0.013**
Lactic acid	**1.141 ± 0.107**	**1.835 ± 0.289**	**df= 18, t= -2.252, P= 0.037**
Acetic acid	1.877 ± 0.341	1.750 ± 0.130	df= 18, t= 0.346, P= 0.733
Propionic acid	0.299 ± 0.033	0.372 ± 0.027	df= 18, t= -1.704, P= 0.106
n-butyric acid	0.865 ± 0.225	0.907 ± 0.209	df= 18, t= -0.137, P= 0.893

The values are the mean ± SEM (n=10).

Bold was statistically significant.

Discussion

The major findings of this study were as follows. First, topical application of IMQ to skin caused psoriasis-like phenotypes in mice. Second, IMQ caused significant alterations in the alpha- and beta-diversity of the microbiota in the intestine and on the skin. The LEfSe algorithm of gut microbiota identified the species *Lactobacillus intestinalis*, *Lactobacillus reuteri*, and *Bacteroides uniformis* as potential gut microbial markers for the IMQ group. Furthermore, the LEfSe algorithm of skin microbiota identified the species *Staphylococcus lentus* as potential skin microbial marker for the IMQ group. Interestingly, correlations for several microbes between the intestine and the skin were observed, suggesting a role of skin–gut–microbiota in IMQ-treated mice. Third, levels of succinic acid and lactic acid in feces increased in the IMQ group compared to control group. Interestingly, we found that the levels of succinic acid (or lactic acid) were correlated with the relative abundance of several microbes in the fecal samples. Finally, the predictive functional analysis of the microbiota of gut and skin showed that IMQ caused alterations in several KEGG pathways. Taken all together, the present data show that topical treatment with IMQ alters the composition of the microbiota in the intestine and on the skin of host.

At the species level, the three *Lactobacillus* microbes such as *Lactobacillus intestinalis*, *Lactobacillus reuteri*, and *Lactobacillus taiwanensis* were significantly higher in the intestine of IMQ-treated mice compared to control mice. A recent study showed that *Lactobacillus intestinalis* and *Lactobacillus reuteri* may be responsible for the depression-like behavior in mice after transplantation of “depression-related microbes” (40). The increased abundance of *Lactobacillus intestinalis, Lactobacillus reuteri* and *Lactobacillus taiwanensis* by IMQ treatment may contribute to the increased levels of lactic acid in the IMQ-treated mice since *Lactobacilli* ferment lactose into lactic acid (41). Collectively, it is likely that increased abundance of *Lactobacillus* bacteria may contribute to increased levels of lactic acid in the host gut although further detailed study is needed. Considering the beneficial actions of *Lactobacillus reuteri* on the host immune system (41,42), it seems that IMQ-induced increases in the abundance of bacteria might reflect a compensatory response in the host. There are many species of *Lactobacillus* which may have beneficial and harmful effects in the host (43).

Nonetheless, future studies are needed to investigate the mechanisms underpinning increases of these *Lactobacillus* bacteria in the intestine of IMQ-treated mice.

Furthermore, we found significant differences for *Bacteroides uniformis, Bacteroides acidifaciens, Bacteroides sartorii, Staphylococcus lentus* and *Parabacteroides distasonis* in the intestine between the two groups. As far as we know, there are no reports showing alterations in these three *Bacteroides* bacteria in IMQ-treated mice and patients with psoriasis. Pretreatment with the antibiotic metronidazole increased the abundance of *Parabacteroides distasonis* in the intestine of IMQ-treated mice (30). In contrast, *Parabacteroides distasonis* were significantly decreased in the patients with psoriasis (44).

At the species level, we found many skin microbes which altered in the IMQ-treated mice (**Table S5**). Importantly, the most abundant microbe on the skin from IMQ-treated mice was *Staphylococcus lentus*, and the abundance of *Staphylococcus lentus* in the IMQ-treated mice were significantly higher than control mice (**Table S5**). *Staphylococcus lentus* are commensal bacterium colonizing the skin of animals and has been associated with infections in animals (45). It seems that high abundance of *Staphylococcus lentus* may play a role in IMQ-induced psoriasis-like symptoms in mice. However, the precise mechanisms underlying high abundance of *Staphylococcus lentus* on the skin of IMQ-treated mice are currently unclear. Further study is needed to examine the role of *Staphylococcus lentus* in psoriasis-like symptom of IMQ-treated mice.

In this study, we found several microbes which altered in the both intestine and skin. Interestingly, we found significant correlations for *Lactobacillus intestinalis*, *Lactobacillus reuteri*, *Lactobacillus taiwanensis,* and *Staphylococcus lentus* between the intestine and the skin. To the best of our knowledge, this is the first report showing the correlations for microbes in both the intestine and the skin, supporting the skin–gut microbiota axis (46,47). From the current data, it is unclear whether changes in gut microbiota can affect skin microbiota or these two phenomena are independent. In this study, we found that topical treatment with IMQ caused increased volume of spleen through systemic inflammation, resulting in abnormal changes in the microbiota composition in the intestine and on the skin of mice. Although the precise mechanisms

underlying the association between the skin and the intestine remain unclear, the current data strongly suggest a role of skin–gut microbiota axis in IMQ-treated mice. Therefore, it is of great interest to investigate whether the composition of microbiota in the intestine and on the skin from patients with psoriasis is altered compared to healthy control subjects.

Succinic acid is produced in large amounts during bacterial fermentation of dietary fiber, and it is considered as a key intermediate in the synthesis of propionic acid (48,49). Interestingly, germ-free mice have little or no detectable levels of succinic acid in feces compared to conventional mice, indicating that gut microbiota are the predominant source for succinic acid. Higher levels of succinic acid may be related with high abundance of *Bacteroides* in fecal samples since succinic acid is produced by primary fermenters such as *Bacteroides* (49). It is also shown that elevated levels of succinic acid in the feces are associated with intestinal inflammation (48,49). Collectively, higher levels of succinic acid in the feces of IMQ-treated mice might be associated with intestinal inflammation although further study is needed.

To understand the role of altered composition of microbiota in the intestine and skin of IMQ-treated mice, we examined the predictable function of the microbiota. The current data show that IMQ treatment may contribute to the altered metabolism (i.e., cardiovascular disease, and endocrine and metabolic disease) induced by gut microbiota. In addition, the current data show that IMQ treatment could produce the altered metabolism (i.e., sphingolipid signaling pathway, coronavirus disease – COVID-19, steroid degradation, and renin secretion) induced by skin microbiota. It is noteworthy that we could detect the altered metabolism of endocrine disease in IMQ-treated mice since the neuroendocrine system plays a role in the skin function (31,32). Furthermore, it is likely that gut microbiota is more complex than skin microbiota since we detected many pathways for gut microbiota compared to skin microbiota. Taken together, it is likely that these KEGG pathways provide a new functional view for understanding the gut and skin microbiota that contribute to psoriasis-like symptoms. Finally, this study has a potential limitation. A future study using antibiotic cocktail is needed to ascertain the correlation between skin microbiota and gut microbiota in IMQ-treated mice.

In conclusion, this study shows that topical treatment with IMQ causes abnormal changes in the microbiota composition in the intestine and on the skin of adult mice, and that levels of succinic acid were associated with the relative abundance of several microbes. Furthermore, we found correlations for several microbes between the intestine and the skin, suggesting a role of skin–gut microbiota in psoriasis.

Materials and Methods

Animals

Female C57BL/6 mice (9 weeks old, weighing 18–21 g, n = 20, Japan SLC Inc., Hamamatsu, Shizuoka, Japan) were used. Mice were housed (5 per cage) under a 12-h/12-h light/dark cycle (lights on between 07:00 and 19:00), with *ad libitum* access to food (CE-2; CLEA Japan, Inc., Tokyo, Japan) and water. The experimental protocol was approved by Chiba University Institutional Animal Care and Use Committee (Permission number: 2-433) (50). This study was carried out in strict accordance with the recommendations in the Guide for the Care and Use of Laboratory Animals of the National Institutes of Health, USA (50). This study was also carried out in compliance with the ARRIVE guidelines. All efforts were made to minimize animal suffering.

Treatment of IMQ and collection of samples

The shaved back skin of mice was treated with 62.5 mg of 5% IMQ cream (Beselna cream; Mochida Pharmaceutical Co., Tokyo, Japan) daily for 5 consecutive days. Control mice were treated similarly with 62.5 mg of white petrolatum (Maruishi Pharmaceutical Co., Osaka, Japan). Skin, fecal and spleen samples were collected on day 6. The clinical skin score was measured on day 1 and day 6. The degree of skin inflammation was scored by cumulative disease severity score, similar to the human Psoriasis Area and Severity Index, but not taking the area into account. Erythema, scaling, and thickening were scored independently from 0 to 4: 0, none; 1, slight; 2, moderate; 3, marked; 4, very marked. The single scores were summed, resulting in a theoretical maximal total score of 12 (27).

Fresh fecal samples of mice were collected from 7:30 to 8:30 on day 6 to exclude any circadian effects on the microbes. The fecal samples were placed into sterilized screw-cap microtubes immediately after defecation, and they were frozen in liquid-

nitrogen immediately. The samples were stored at −80°C until use (51).

Skin swabs from the shaved back skin of IMQ-treated mice or control mice were put into extraction tube containing a solution (0.15 M NaCl and 0.1% Tween20) and rotated for at least 20 times. After squeezing as much liquid as possible from the swab by pushing the swabs against the sides of the tubes, the tubes were stored at −80°C until analysis.

Histology

Back skin samples from control and IMQ-treated groups were collected and fixed in 10% formalin (FUJIFILM Wako Pure Chemical Corp.). Staining with hematoxylin and eosin (HE) was performed at Biopathology Institute Co., Ltd (Kunisaki, Oita, Japan). Back skin samples were embedded in paraffin, and sections of 3 μm were prepared and subjected to HE staining. Representative images of two groups were obtained using a Keyence BZ-9000 Generation II microscope (Osaka, Japan)

16S rRNA analysis

The DNA extractions from the fecal and skin samples and 16S rRNA sequencing analyses were performed by MyMetagenome Co., Ltd. (Tokyo, Japan), as reported previously (40,50,51,52). DNA extraction from mouse samples and purification were performed according to the method of the previous report (53,54). The 16S rRNA analysis of samples was performed as previously reported (53,54). Briefly, PCR was performed using 27Fmod 5′-AGRGTTTGATYMTGGCTCAG-3′ and 338R 5′-TGCTGCCTCCCGTAGGAGT-3′ to amplify the V1–V2 region of the bacterial 16S rRNA gene. The 16S amplicons were then sequenced using MiSeq according to the Illumina protocol. Taxonomic assignment of OTUs was made by similarity searches against the Ribosomal Database Project and the National Center for Biotechnology Information genome database using the GLSEARCH program.

Alpha diversity was used to analyze the species diversity, composed of richness and evenness, within a sample through three indices including the observed OTU, ACE, and Shannon indices (55). Beta diversity was used to measure differences of species diversity among samples, including PCA, PCoA with ANOSIM. Differences in bacterial taxa between groups at the species or higher level (depending on the taxon annotation) were calculated based on linear discriminant analysis (LDA) effect size (LEfSe) using

LEfSe software (LDA score > 4.0, P < 0.05) (https://www.omicstudio.cn/tool/) (56).

Prediction of functional profiles of gut microbiota using PICRUSt

Using the 16S rRNA gene sequencing data and KEGG (Kyoto Encyclopedia of Genes and Genome) orthology (http://www.kegg.jp/kegg1.html) (57), we performed PICRUSt (Phylogenetic Investigation of Communities by Reconstruction of Unobserved States) analysis and STAMP (Statistical Analysis of Metagenomic Profiles) software v2.1.3 (http://kiwi.cs.dal.ca/Software/STAMP) for the functional prediction of microbiota in the intestine and skin (55,58,59).

Measurement of short-chain fatty acid (SCFA) levels

Concentrations of SCFAs (i.e., acetic acid, propionic acid, butyric acid, lactic acid, succinic acid) in fecal samples were measured at TechnoSuruga Laboratory, Co., Ltd. (Shizuoka, Japan), as reported previously (50,51,55,60). The data of SCFAs were shown as milligrams per gram of feces.

Statistical analysis

Data are shown as the mean ± standard error of the mean (SEM). Alpha-diversity of the gut and skin microbiota were analyzed using Mann-Whitney U-test. Analysis of beta-diversity of the gut and skin microbiota including PCA of OTU level and PCoA of weighted UniFrac distances were performed based on ANOSIM by R package vegan (2.5.4) (https://CRAN.R-project.org/package=vegan) (61). Data for SCFA levels were analyzed using Student t-test. Correlations between SCFAs and the relative bacterial abundance were analyzed using Spearman's correlation analysis. Correlations between the relative abundance of bacteria in the skin and intestine were also analyzed using Spearman's correlation analysis. $P < 0.05$ was considered statistically significant.

References

1. Michalek, I.M., Loring, B. & John. S.M. A systematic review of worldwide epidemiology of psoriasis. *J. Eur. Acad. Dermatol. Venereol.* **31**, 205-212 (2017).
2. Boehncke, W.H. & Schön, M.P. Psoriasis. *Lancet* **386**, 983-994 (2015).
3. Armstrong, A.W. & Read, C. Pathophysiology, clinical presentation, and treatment of psoriasis: a review. *JAMA* **323**, 1945-1960 (2020).
4. Geale, K., Henriksson, M., Jokinen, J. & Schmitt-Egenolf, M. Association of skin psoriasis and somatic comorbidity with the development of psychiatric illness in a Nationwide Swedish Study. *JAMA Dermatol.* **156**, 795-804 (2020).
5. Kleyn, C.E. *et al*. Psoriasis and mental health workshop report: exploring the links between psychosocial factors, psoriasis, neuroinflammation and cardiovascular disease risk. *Acta. Derm .Venereol.* **100**, adv00020 (2020).
6. Nestle, F.O., Kaplan, D.H. & Barker, J. Psoriasis. *N. Engl. J. Med.* **361**, 496-509 (2009).
7. Round, J.L. & Mazmanian, S.K. The gut microbiota shapes intestinal immune responses during health and disease. *Nat. Rev. Immunol.* **9**, 313-323 (2009).
8. Cho, I. & Blaser, M.J. The human microbiome: at the interface of health and disease. *Nat. Rev. Genet.* **13**, 260-272 (2012).
9. Shreiner, A.B., Kao, J.Y. & Young, V.B. The gut microbiome in health and in disease. *Curr. Opin. Gastroenterol.* **31**, 69-75 (2015).
10. Althani, A.A. *et al*. Human microbiome and its association with health and diseases. *J. Cell Physiol.* **231**, 1688-1694 (2016).
11. Fung, T.C., Olson, C.A. & Hsiao, E.Y. Interactions between the microbiota, immune and nervous systems in health and disease. *Nat. Neurosci.* **20**, 145-155 (2017).
12. Young, V.B. The role of microbiome in human health and disease: an introduction for clinicians. *BMJ* **356**, j831 (2017).
13. Cryan, J.F. *et al*. The microbiota-gut-brain axis. *Physiol. Rev.* **99**, 1877-2013 (2019).
14. Chen, L. *et al*. Skin and Gut Microbiome in psoriasis: gaining insight into the pathophysiology of it and finding novel therapeutic strategies. *Front. Microbiol.* **11**,

589726 (2020).

15. Codoñer, F.M. *et al*. Gut microbial composition in patients with psoriasis. *Sci. Rep.* **8**, 3812 (2018).
16. Hidalgo-Cantabrana, C. *et al*. Gut microbiota dysbiosis in a cohort of patients with psoriasis. *Br. J. Dermatol.* **181**, 1287-1295 (2019).
17. Shapiro, J., Cohen, N.A., Shalev, V., Uzan, A., Koren, O. & Maharshak, N. Psoriatic patients have a distinct structural and functional fecal microbiota compared with controls. *J. Dermatol.* **46**, 595-603 (2019).
18. Dei-Cas, I., Giliberto, F., Luce, L., Dopazo, H. & Penas-Steinhardt, A. Metagenomic analysis of gut microbiota in non-treated plaque psoriasis patients stratified by disease severity: development of a new Psoriasis-Microbiome Index. *Sci. Rep.* **10**, 12754 (2020).
19. Sikora, M. *et al*. Gut microbiome in psoriasis: An updated review. *Pathogens* **9**, 463 (2020).
20. Fahlén, A., Engstrand, L., Baker, B.S., Powles, A. & Fry, L. Comparison of bactrial microbiota in skin biosies from normal and psoriatic skin. *Arch. Dermatol. Res.* **304**, 15-22 (2012).
21. Alekseyenko, A.V. *et al*. Community differentiation of the cutaneous microbiota in psoriasis. *Microbiome* **1**, 31 (2013).
22. Zákostelská, Z. et al. Intestinal microbiota promotes psoriasis-like skin inflammation by enhancing Th17 response**.** *PLoS One* **11**, e0159539 (2016).
23. Assarsson, M., Duvetorp, A., Dienus, O., Söderman, J. & Seifert, O. Significant changes in the skin microbiome in patients with chronic plaque psoriasis after treatment with narrowband ultraviolet B. *Acta. Derm. Venereol.* **98**, 428-436 (2018).
24. Chang, H.W, *et al*. Alteration of the cutaneous microbiome in psoriasis and potential role in Th17 polarization. *Microbiome* **6**, 154 (2018).
25. Fyhrquist, N. *et al*. Microbe-host interplay in atopic dermatitis and psoriasis. *Nat. Commun.* **10**, 4703 (2019).
26. Flutter, B. & Nestle, F.O. TLRs to cytokines: Mechanistic insights from the imiquimod mouse model of psoriasis. *Eur. J. Immunol.* **43**, 3138-3146 (2013).
27. van der Fits, L. *et al*. Imiquimod-induced psoriasis-like skin inflammation in mice

is mediated via the IL-23/IL-17 axis**.** *J. Immunol.* **182**, 5836-5845 (2009).

28. Zanvit, P. *et al.* Antibiotics in neonatal life increase murine susceptibility to experimental psoriasis. *Nat. Commun.* **6**, 8424 (2015).
29. Kiyohara, H. *et al*. Toll-like receptor 7 agonist-induced dermatitis causes severe dextran sulfate sodium colitis by altering the gut microbiome and immune cells. *Cell Mol. Gastroenterol. Hepatol.* **7**, 135-156 (2018).
30. Stehlikova, Z. *et al*. Crucial role of microbiota in experimental psoriasis revealed by a gnotobiotic mouse model. *Front. Microbiol.* **10**, 236 (2019).
31. Slominski, A. & Wortsman, J. Neuroendocrinology of the skin. *Endocr. Rev.* **21**, 457-487 (2000).
32. Slominski, A.T., Manna, P.R. & Tuckey, R.C. On the role of skin in the regulation of local and systemic steroidogenic activities. *Steroids* **103**, 72-88 (2015).
33. den Besten, G., van Eunen, K., Groen, A.K., Venema, K., Reijngoud, D.J. & Bakker, B.M. The role of short-chain fatty acids in the interplay between diet, gut microbiota, and host energy metabolism. *J. Lipid Res.* **54**, 2325-2340 (2013).
34. Morrison, D.J. & Preston, T. Formation of short chain fatty acids by the gut microbiota and their impact on human metabolism. *Gut Microbes* **7**, 189-200 (2016).
35. Chambers, E.S., Preston, T., Frost, G. & Morrison, D.J. Role of gut microbiota-generated short-chain fatty acids in metabolic and cardiovascular health. *Curr. Nutr. Rep.* **7**, 198-206 (2018).
36. Dalile, B., Van Oudenhove, L., Vervliet, B. & Verbeke, K. The role of short-chain fatty acids in microbiota-gut-brain communication. *Nat. Rev. Gastroenterol. Hepatol.* **16**, 461-478 (2019).
37. Qin, S. *et al*. Endogenous n-3 polyunsaturated fatty acids protect against imiquimod-induced psoriasis-like inflammation via the IL-17/IL-23 axis. *Mol. Med. Rep.* 9, 2097-2104 (2014).
38. Lee, J., Song, K., Hiebert, P., Werner, S., Kim, T.G. & Kim, Y.S. Tussilagonone ameliorates psoriatic fearures in keratinocytes and imiquimod-induced psoriasis-like lesions in mice via NRF2 activation. *J. Invbest. Dermatol.* **140**, 1223-1232 (2020).

39. Schwarz, A., Philippsen, R. & Schwarz, T. Induction of regulatory T cells and correction of cytokine disbalance by short-chain fatty acids: Implications for psoriasis therapy. *J. Invest. Dermatol.* **141**, 95-104 (2021).
40. Wang, S. *et al*. Ingestion of *Lactobacillus intestinalis* and *Lactobacillus reuteri* causes depression- and anhedonia-like phenotypes in antibiotic-treated mice via the vagus nerve. *J. Neuroinflamm.* **17**, 241 (2020).
41. Fine, R.L., Mubiru, D.L. & Kriegel, M.A. Friend or foe? *Lactobacillus* in the context of autoimmune disease. *Adv. Immunol.* **146**, 29-56 (2020).
42. Mu, Q., Tavella, V.J. & Luo, X.M. Role of *Lactobacillus reuteri* in human health and diseases. *Front. Microbiol.* **9**, 757 (2018).
43. Masood, M.I., Qadir, MI., Shirazi, J.H. & Khan, I.U. Beneficial effects of lactic acid bacteria on human being. *Crit. Rev. Microbiol.* **37**, 91-98 (2010).
44. Shapiro, J. *et al*. Psoriatic patients have a distinct structural and functional fecal microbiota compared with controls. *J. Dermatol.* **46**, 595-603 (2019).
45. Nemeghaire, S. *et al*. The ecological importance of the *Staphylococcus sciuri* species group as a reservor for resistance and virulence genes. *Vet. Microbiol.* **171**, 342-356 (2014).
46. Chen, G. *et al*. Gut-brain-skin axis in psoriasis: a review. Dermatol. Ther (Heidelb) 2020 Nov 18. doi: 10.1007/s13555-020-00466-9.
47. Van Splunter, M. *et al*. Mechanisms underlying the skin-gut cross talk in the development of IgE-mediated food allergy. *Nutrients* **12**, 3830 (2020).
48. Connors, J., Dawe, N. & Van Limbergen, J. The role of succinate in the regulation of intestinal inflammation. *Nutrients* **11**, 25 (2018).
49. Fernández-Veledo, S. & Vendrell, J. Gut microbiota-derived succinate: Friend or foe in human metabolic diseases? *Rev. Endocr. Metab. Disord.* **20**, 439-447 (2019).
50. Wang, S., Qu, Y., Chang, L., Pu, Y., Zhang, K. & Hashimoto, K. Antibiotic-induced microbiome depletion is associated with resilience in mice after chronic social defeat stress. *J. Affect. Disord.* **260**, 448-457 (2020).
51. Pu, Y. *et al*. A role of the subdiaphragmatic vagus nerve in depression-like phenotypes in mice after fecal microbiota transplantation from *Chrna7* knock-out mice with depression-like phenotypes. *Brain Behav. Immun.* **94**, 318-326 (2021).

52. Zhang, J., Ma, L., Chang, L., Pu, Y., Qu, Y. & Hashimoto, K. A key role of the subdiaphragmatic vagus nerve in the depression-like phenotype and abnormal composition of gut microbiota in mice after lipopolysaccharide administration. *Transl. Psychiatry* **10**, 186 (2020).
53. Kim, S.W. et al. Robustness of gut microbiota of healthy adults in response to probiotic intervention revealed by high-throughput pyrosequencing. *DNA Res.* **20**, 241-253 (2013).
54. Shibagaki, N. *et al.* Aging-related changes in the diversity of women's skin microbiomes associated with oral bacteria. *Sci. Rep.* **7,** 10567 (2017).
55. Wei, Y. *et al*. Abnormalities of the composition of the gut microbiota and short-chain fatty acids in mice after splenectomy. *Brain Beahv. Imun. Health* **11**, 100198 (2021).
56. Segata, N. *et al*. Metagenomic biomarker discovery and explanation. *Genome Biol.* **12**, R60 (2011).
57. Kanehisa, M., Furumichi, M., Sato, Y., Ishiguro-Watanabe, M., Tanabe, M. KEGG: integrating viruses and cellular organisms. *Nucleic Acid Res.* **49 (D1)**, D545-D551.
58. Langille, M.G. *et al*. Predictive functional profiling of microbial communities using 16S rRNA marker gene sequences. *Nat. Biotechnol.* **31**, 814-821 (2013).
59. Parks, D.H., Tyson, G.W., Hugenholtz, P. & Beiko, R.G. STAMP: statistical analysis of taxonomic and functional profiles. *Bioinformatics* **30**, 3123-3124 (2014).
60. Zhang, K. *et al*. Abnormal composition of gut microbiota is associated with resilience versus susceptibility to inescapable electric stress. *Transl. Psychiatry* **9**, 231 (2019).
61. Xin, Y. & Sun, J. Hypothesis testing and statistical analysis of microbiome. *Genes Diseases* **4**, 138-148 (2017).

Supplemental Information

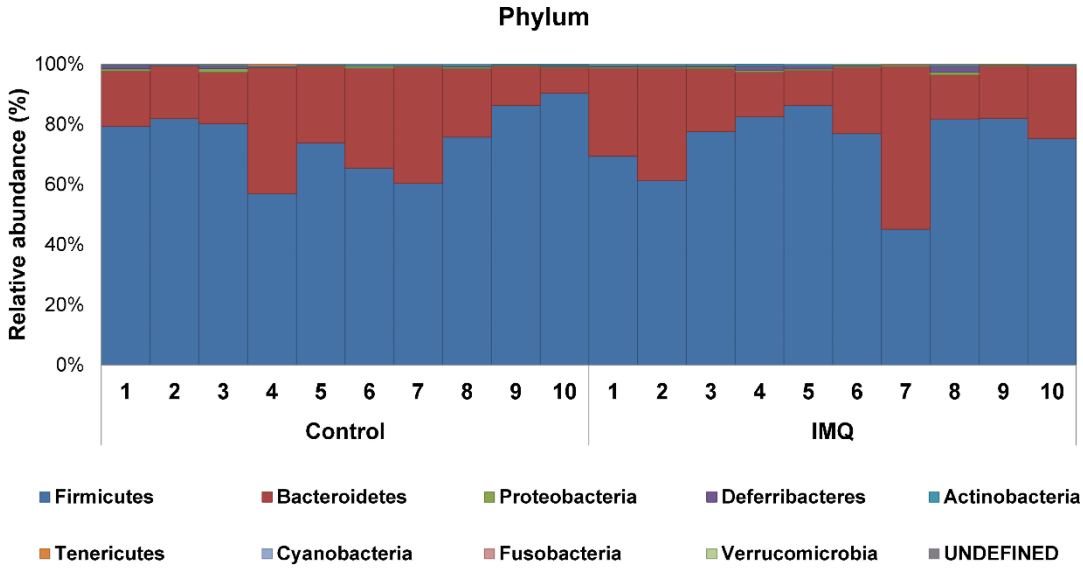

Figure S1. The composition in the gut microbiota at the levels of phylum

The relative abundances of gut microbiome at phylum level in fecal samples of the control and IMQ groups. There were no changes for microbes between the two groups.

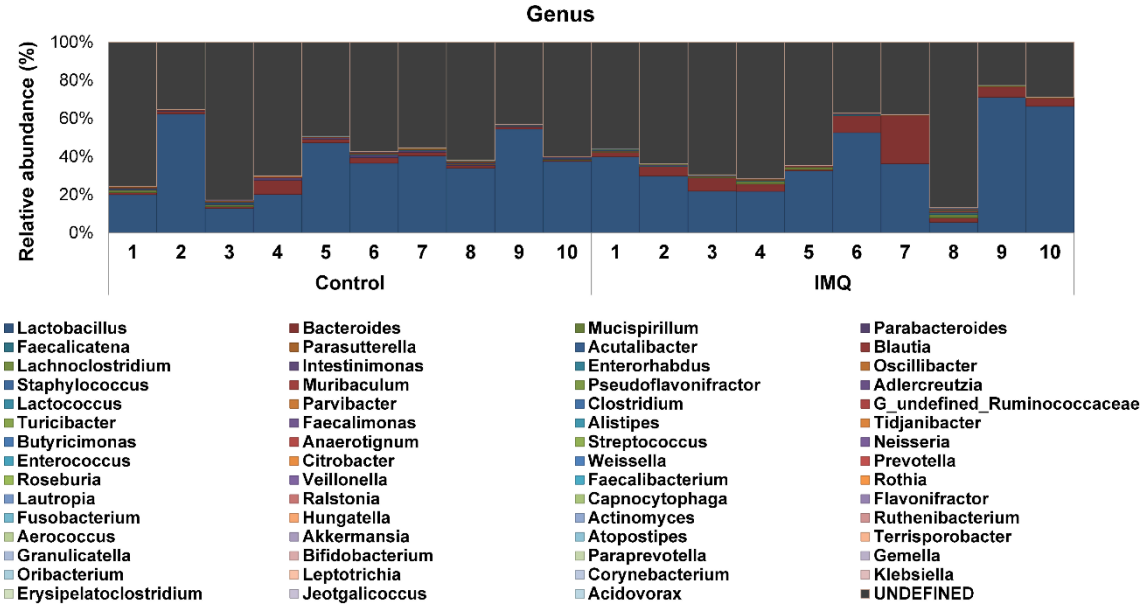

Figure S2. The composition in the gut microbiota at the levels of genus

The relative abundances of gut microbiome at genus level in fecal samples of the control and IMQ groups. There were significantly ($P < 0.001$) changes for *Parabacteroides*, *Staphylococcus*, and *Alistipes* between the two groups (**Table S1**).

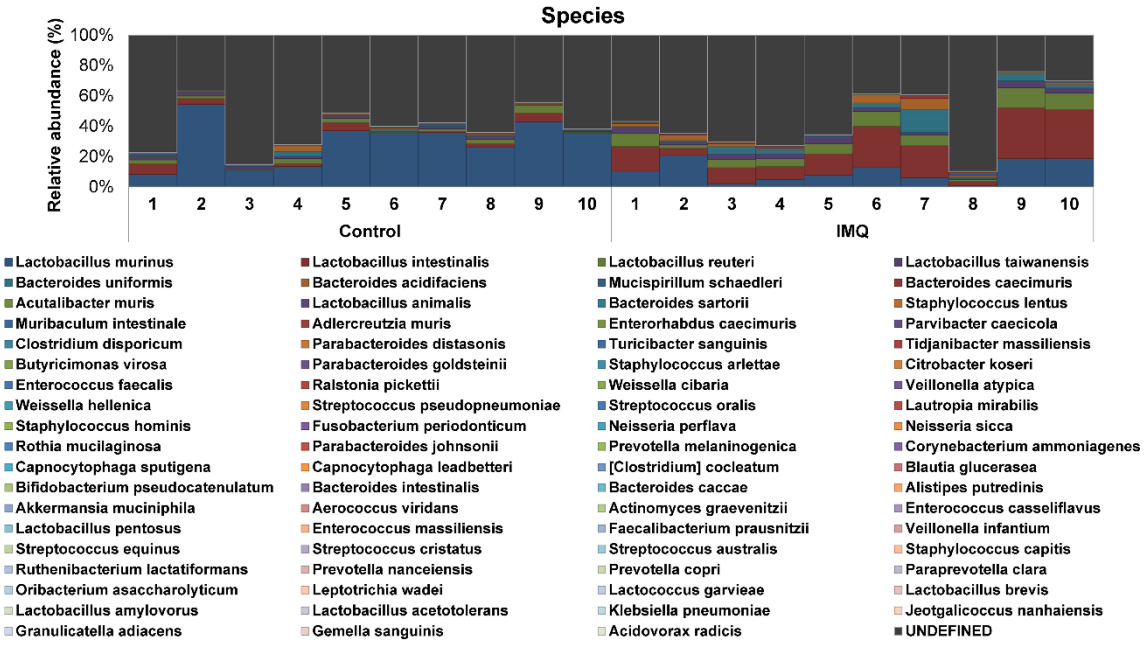

Figure S3. The composition in the gut microbiota at the levels of species

The relative abundances of gut microbiome at species level in fecal samples of the control and IMQ groups. There were significantly changes for several microbiome between the two groups (**Table S2**).

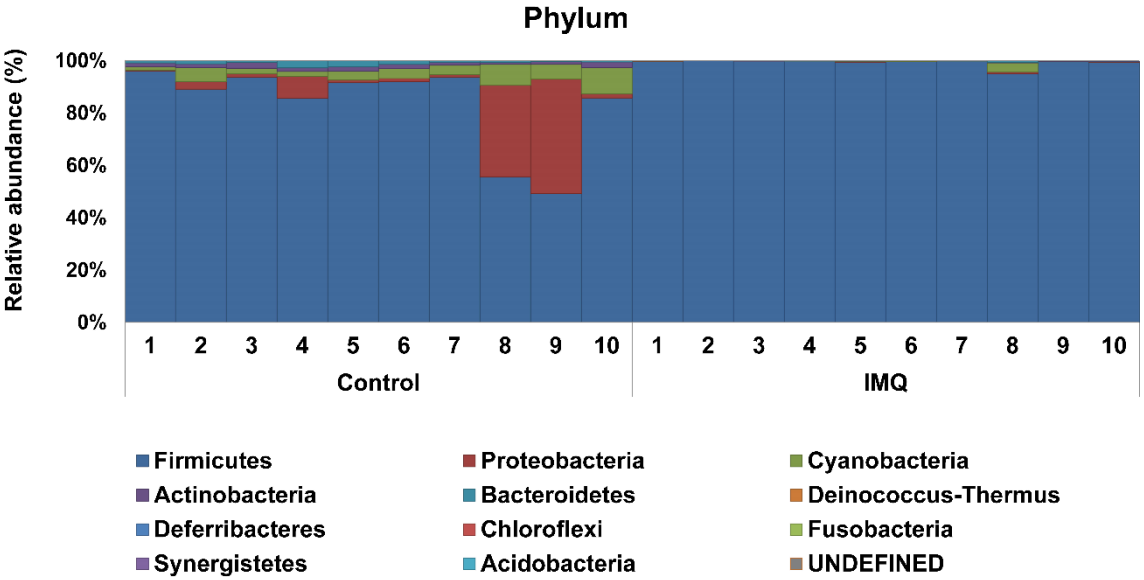

Figure S4. The composition in the skin bacteria at the levels of phylum

The relative abundances of skin microbiome at phylum level in skin samples of the control and IMQ groups. There were significantly ($P < 0.001$) changes for *Firmicutes*, *Proteobacteria, Cyanobacteria*, *Actinobacteria* and *Bacteroidetes* between the two groups (**Table S3**).

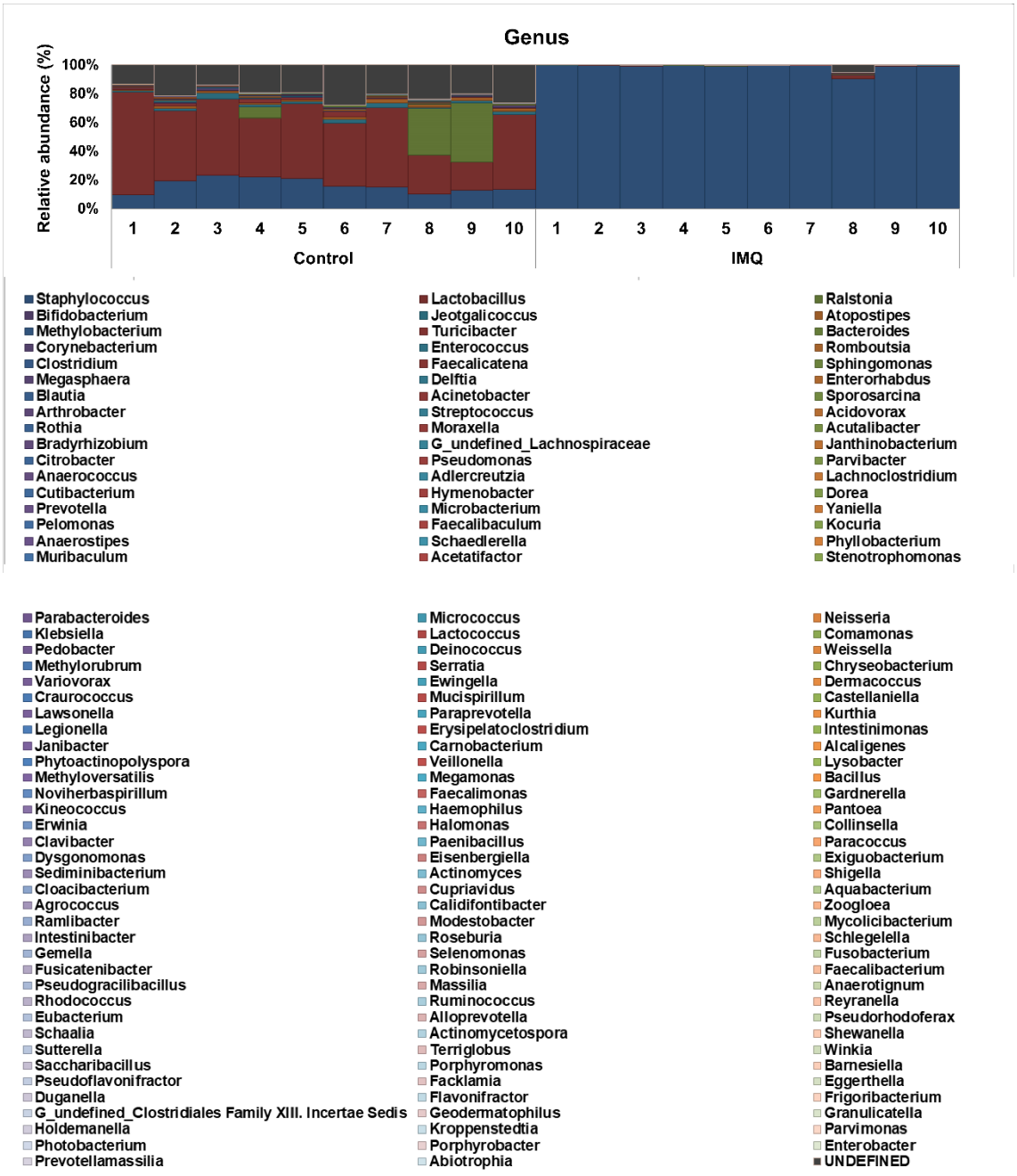

Figure S5. The composition in the skin microbiota at the levels of genus

The relative abundances of skin microbiome at genus level in skin samples of the control and IMQ groups. There were significantly changes for sixteen microbes between the two groups (**Table S4**).

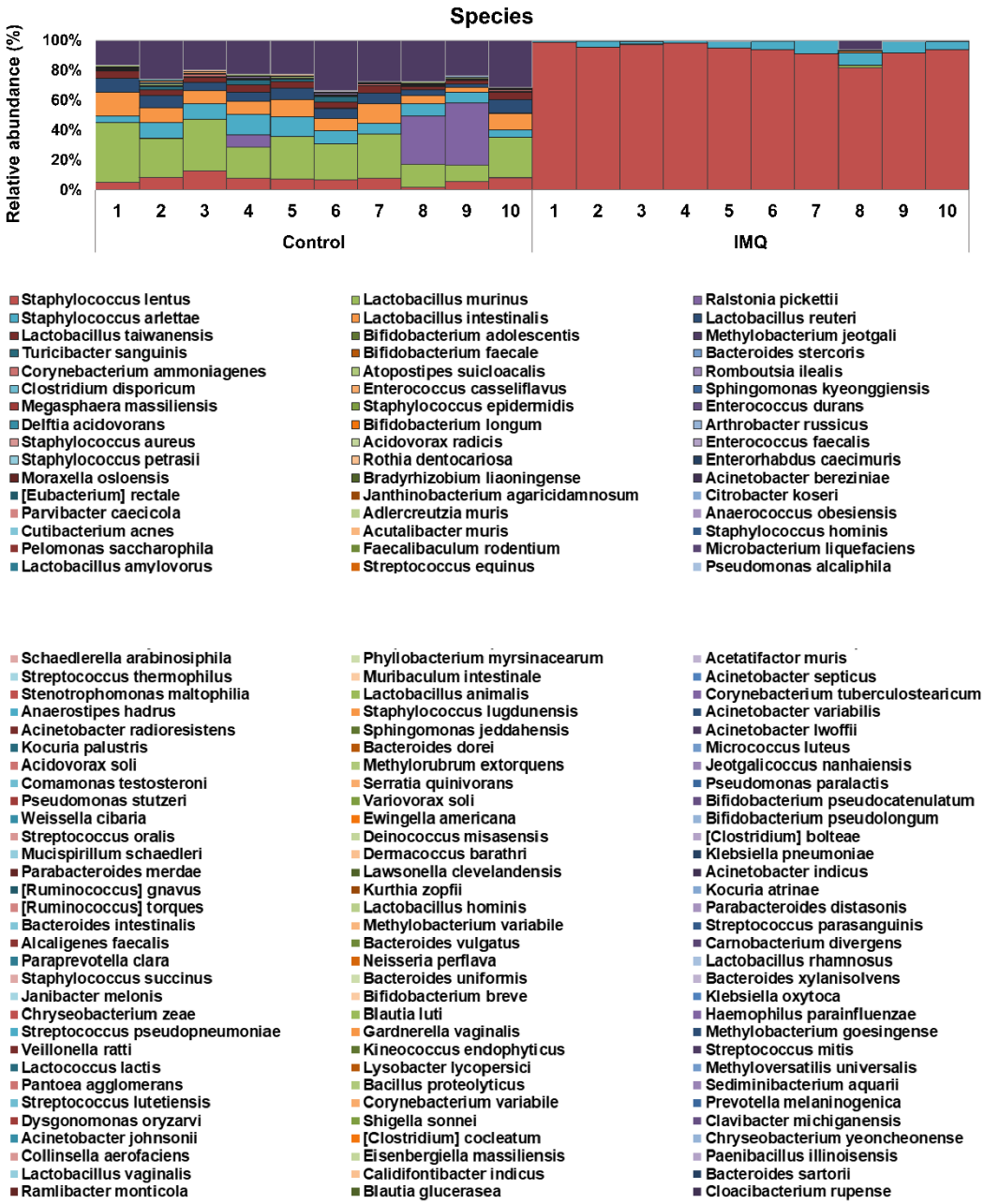
Species
Relative abundance (%)
100%
80%
60%
40%
20%
0%
1 2 3 4 5 6 7 8 9 10
Control
1 2 3 4 5 6 7 8 9 10
IMQ
Staphylococcus lentus
Staphylococcus arlettae
Lactobacillus taiwanensis
Turicibacter sanguinis
Corynebacterium ammoniagenes
Clostridium disporicum
Megasphaera massiliensis
Delftia acidovorans
Staphylococcus aureus
Staphylococcus petrasii
Moraxella osloensis
[Eubacterium] rectale
Parvibacter caecicola
Cutibacterium acnes
Pelomonas saccharophila
Lactobacillus amylovorus
Lactobacillus murinus
Lactobacillus intestinalis
Bifidobacterium adolescentis
Bifidobacterium faecale
Atopostipes suicloacalis
Enterococcus casseliflavus
Staphylococcus epidermidis
Bifidobacterium longum
Acidovorax radicis
Rothia dentocariosa
Bradyrhizobium liaoningense
Janthinobacterium agaricidamnosum
Adlercreutzia muris
Acutalibacter muris
Faecalibaculum rodentium
Streptococcus equinus
Ralstonia pickettii
Lactobacillus reuteri
Methylobacterium jeotgali
Bacteroides stercoris
Romboutsia ilealis
Sphingomonas kyeonggiensis
Enterococcus durans
Arthrobacter russicus
Enterococcus faecalis
Enterorhabdus caecimuris
Acinetobacter bereziniae
Citrobacter koseri
Anaerococcus obesiensis
Staphylococcus hominis
Microbacterium liquefaciens
Pseudomonas alcaliphila
Schaedlerella arabinosiphila
Streptococcus thermophilus
Stenotrophomonas maltophilia
Anaerostipes hadrus
Acinetobacter radioresistens
Kocuria palustris
Acidovorax soli
Comamonas testosteroni
Pseudomonas stutzeri
Weissella cibaria
Streptococcus oralis
Mucispirillum schaedleri
Parabacteroides merdae
[Ruminococcus] gnavus
[Ruminococcus] torques
Bacteroides intestinalis
Alcaligenes faecalis
Paraprevotella clara
Staphylococcus succinus
Janibacter melonis
Chryseobacterium zeae
Streptococcus pseudopneumoniae
Veillonella ratti
Lactococcus lactis
Pantoea agglomerans
Streptococcus lutetiensis
Dysgonomonas oryzarvi
Acinetobacter johnsonii
Collinsella aerofaciens
Lactobacillus vaginalis
Ramlibacter monticola
Phyllobacterium myrsinacearum
Muribaculum intestinale
Lactobacillus animalis
Staphylococcus lugdunensis
Sphingomonas jeddahensis
Bacteroides dorei
Methylorubrum extorquens
Serratia quinivorans
Variovorax soli
Ewingella americana
Deinococcus misasensis
Dermacoccus barathri
Lawsonella clevelandensis
Kurthia zopfii
Lactobacillus hominis
Methylobacterium variabile
Bacteroides vulgatus
Neisseria perflava
Bacteroides uniformis
Bifidobacterium breve
Blautia luti
Gardnerella vaginalis
Kineococcus endophyticus
Lysobacter lycopersici
Bacillus proteolyticus
Corynebacterium variabile
Shigella sonnei
[Clostridium] cocleatum
Eisenbergiella massiliensis
Calidifontibacter indicus
Blautia glucerasea
Acetatifactor muris
Acinetobacter septicus
Corynebacterium tuberculostearicum
Acinetobacter variabilis
Acinetobacter lwoffii
Micrococcus luteus
Jeotgalicoccus nanhaiensis
Pseudomonas paralactis
Bifidobacterium pseudocatenulatum
Bifidobacterium pseudolongum
[Clostridium] bolteae
Klebsiella pneumoniae
Acinetobacter indicus
Kocuria atrinae
Parabacteroides distasonis
Streptococcus parasanguinis
Carnobacterium divergens
Lactobacillus rhamnosus
Bacteroides xylanisolvens
Klebsiella oxytoca
Haemophilus parainfluenzae
Methylobacterium goesingense
Streptococcus mitis
Methyloversatilis universalis
Sediminibacterium aquarii
Prevotella melaninogenica
Clavibacter michiganensis
Chryseobacterium yeoncheonense
Paenibacillus illinoisensis
Bacteroides sartorii
Cloacibacterium rupense

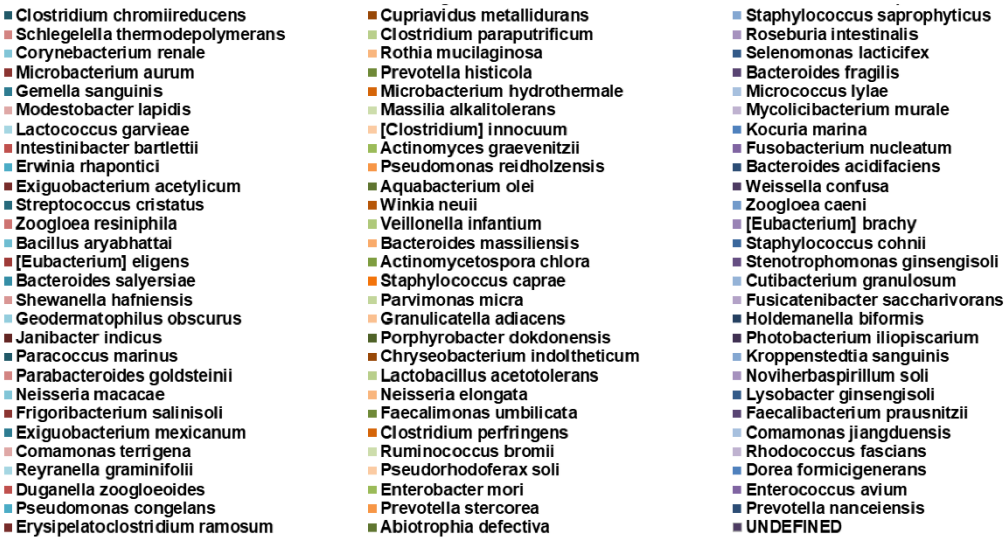

Figure S6. The composition in the skin microbiota at the levels of species

The relative abundances of skin microbiome at species level in skin samples of the control and IMQ groups. There were significantly changes for fourteen microbes between the two groups (**Table S5**).

Table S1. The gut bacteria that significantly differ between control and IMQ groups at the genus level.

Genus	Relative abundance in Control (%)	Relative abundance in IMQ (%)	Mann-Whitney U test
Bacteroides	2.012 ± 0.627	6.429 ± 2.188	U= 81, P= 0.019
Parabacteroides	0.689 ± 0.131	0.040 ± 0.014	U= 0, P= 0.000
Staphylococcus	0.017 ± 0.005	0.081 ± 0.017	U= 93, P= 0.000
Faecalimonas	0.028 ± 0.006	0.010 ± 0.003	U= 21, P= 0.029
Alistipes	0.030 ± 0.008	0.001 ± 0.001	U= 6, P= 0.000

The values are the mean ± SEM (n=10).

Table S2. The gut bacteria that significantly differ between control and IMQ groups at the species level.

Species	Relative abundance in Control (%)	Relative abundance in IMQ (%)	Mann-Whitney U test
Lactobacillus murinus	30.099 ± 4.761	10.354 ± 2.291	U= 12, P= 0.003
Lactobacillus intestinalis	2.700 ± 0.802	17.062 ± 3.457	U= 93, P= 0.000
Lactobacillus reuteri	2.139 ± 0.480	7.020 ± 1.166	U= 86, P= 0.005
Lactobacillus taiwanensis	1.324 ± 0.274	2.960 ± 0.402	U= 86, P= 0.005
Bacteroides uniformis	0.760 ± 0.286	3.460 ± 1.379	U= 79, P= 0.029
Bacteroides acidifaciens	0.980 ± 0.336	2.531 ± 0.711	U= 83, P= 0.011
Bacteroides sartorii	0.105 ± 0.019	0.009 ± 0.004	U= 3.5, P= 0.000
Staphylococcus lentus	0.003 ± 0.002	0.079 ± 0.017	U= 100, P= 0.000
Parabacteroides distasonis	0.047 ± 0.014	0.001 ± 0.001	U= 6.5, P= 0.000

The values are the mean ± SEM (n=10).

Table S3. The skin bacteria that significantly differ between control and IMQ groups at the phylum.

Phylum	Relative abundance in Control (%)	Relative abundance in IMQ (%)	Mann-Whitney U test
Firmicutes	83.270 ± 5.256	99.242 ± 0.477	U= 99, P= 0.000
Proteobacteria	9.636 ± 5.037	0.137 ± 0.073	U= 1, P= 0.000
Cyanobacteria	4.498 ± 0.884	0.432 ± 0.333	U= 3.5, P= 0.000
Actinobacteria	1.520 ± 0.138	0.065 ± 0.029	U= 0, P= 0.000
Bacteroidetes	1.048 ± 0.267	0.122 ± 0.051	U= 5, P= 0.000

The values are the mean ± SEM (n=10).

Table S4. The skin bacteria that significantly differ between control and IMQ groups at the genus level.

Genus	Relative abundance in Control (%)	Relative abundance in IMQ (%)	Mann-Whitney U test
Staphylococcus	16.200 ± 1.551	98.513 ± 0.914	U= 100, P= 0.000
Lactobacillus	46.420 ± 4.652	0.413 ± 0.287	U= 0, P= 0.000
Jeotgalicoccus	2.011 ± 0.331	0.038 ± 0.034	U= 0, P= 0.000
Atopostipes	1.637 ± 0.187	0.044 ± 0.040	U= 0, P= 0.000
Turicibacter	1.299 ± 0.373	0.009 ± 0.006	U= 0, P= 0.000
Corynebacterium	0.808 ± 0.102	0.020 ± 0.018	U= 0, P= 0.000
Enterococcus	0.326 ± 0.115	0.016 ± 0.009	U= 3.5, P= 0.000
Clostridium	0.351 ± 0.079	0.004 ± 0.002	U= 0, P= 0.000
Faecalicatena	0.263 ± 0.049	0.001 ± 0.001	U= 0, P= 0.000
Sphingomonas	0.030 ± 0.008	0.000 ± 0.000	U= 5, P= 0.000
Enterorhabdus	0.144 ± 0.023	0.001 ± 0.001	U= 0, P= 0.000
Acinetobacter	0.069 ± 0.015	0.002 ± 0.002	U= 1, P= 0.000
Sporosarcina	0.106 ± 0.024	0.002 ± 0.002	U= 1, P= 0.000
Acutalibacter	0.053 ± 0.011	0.000 ± 0.000	U= 0, P= 0.000
Parvibacter	0.044 ± 0.008	0.000 ± 0.000	U= 5, P= 0.000
Adlercreutzia	0.042 ± 0.011	0.000 ± 0.000	U= 5, P= 0.000

The values are the mean ± SEM (n=10).

Table S5. The skin bacteria that significantly differ between control and IMQ groups at the species level.

Species	Relative abundance in Control (%)	Relative abundance in IMQ (%)	Mann-Whitney U test
Staphylococcus lentus	7.138 ± 0.869	93.547 ± 1.534	U= 100, P= 0.000
Lactobacillus murinus	25.643 ± 2.708	0.191 ± 0.124	U= 0, P= 0.000
Lactobacillus intestinalis	9.621 ± 1.180	0.118 ± 0.092	U= 0, P= 0.000
Lactobacillus reuteri	6.543 ± 0.693	0.046 ± 0.035	U= 0, P= 0.000
Lactobacillus taiwanensis	4.021 ± 0.326	0.044 ± 0.032	U= 0, P= 0.000
Turicibacter sanguinis	1.299 ± 0.373	0.009 ± 0.006	U= 0, P= 0.000
Corynebacterium ammoniagenes	0.791 ± 0.103	0.020 ± 0.018	U= 0, P= 0.000
Atopostipes suicloacalis	0.549 ± 0.066	0.002 ± 0.001	U= 0, P= 0.000
Clostridium disporicum	0.348 ± 0.078	0.002 ± 0.001	U= 0, P= 0.000
Enterococcus faecalis	0.068 ± 0.019	0.001 ± 0.001	U= 0, P= 0.000
Enterorhabdus caecimuris	0.058 ± 0.012	0.001 ± 0.001	U= 0, P= 0.000
Parvibacter caecicola	0.044 ± 0.008	0.000 ± 0.000	U= 5, P= 0.000
Adlercreutzia muris	0.042 ± 0.011	0.000 ± 0.000	U= 5, P= 0.000
Acutalibacter muris	0.035 ± 0.010	0.000 ± 0.000	U= 5, P= 0.000

The values are the mean ± SEM (n=10).

Part-2

Effects of splenectomy on skin inflammation and psoriasis-like phenotype of imiquimod-treated mice

Abstract

Imiquimod (IMQ) is widely used as animal model of psoriasis, a chronic inflammatory skin disorder. Although topical application of IMQ to back skin causes splenomegaly in mice, how the spleen affects the psoriasis-like phenotype of IMQ-treated mice remains unclear. In this study, we analyzed the cellular composition of spleen and measured metabolites in blood of IMQ-treated mice. We also investigated whether splenectomy influences the degree of skin inflammation and pathology in IMQ-treated mice. Flow cytometry showed that the numbers of $CD11b^{+}Ly6c^{+}$ neutrophils, $Ter119^{+}$ proerythroblasts, $B220^{+}$ B cells, $F4/80^{+}$ macrophages, and $CD11c^{+}$ dendritic cells in the spleen were significantly higher in IMQ-treated mice compared to control mice. An untargeted metabolomics analysis of blood identified 14 metabolites, including taurine and 2,6-dihydroxybenzoic acid, whose levels distinguished the two groups. The composition of cells in the spleen and blood metabolites positively correlated with the weight of the spleen. However, splenectomy did not affect IMQ-induced psoriasis-like phenotypes compared with sham-operated mice, although splenectomy increased the expression of interleukin-17A mRNA in the skin of IMQ-treated mice. These data suggest that the spleen does not play a direct role in the development of psoriasis-like phenotype on skin of IMQ-treated mice, though IMQ causes splenomegaly.

Keywords: Imiquimod; Splenectomy; Metabolomics analysis; Flow Cytometry; Psoriasis

Introduction

Psoriasis is an autoimmune disease that causes raised plaques and scaly patches on the skin. Yet psoriasis-induced inflammation could harm other organs: patients with psoriasis have a high risk for systemic comorbidities, including psoriatic arthritis, inflammatory bowel diseases, obesity, diabetes, and cardiovascular diseases. For example, approximately 30% of patients with psoriasis develop psoriatic arthritis (1). Data from immunological and genetic studies suggest that interleukin-17 (IL-17) and IL-23 govern crosstalk between the innate and adaptive immune systems in a feed-forward amplification of psoriasis inflammation (2-4). Although excessive activation of the immune system plays a crucial role in the pathogenesis of psoriasis, the precise mechanisms underlying this disease remain elusive (2-8).

Imiquimod (IMQ), a Toll-like receptor 7 agonist, has been used as a rodent model of psoriasis (9,10). It is also suggested that the skin serves as a peripheral neuroendocrine tissue (11,12). Topical application of IMQ to back skin causes splenomegaly in rodents (9, 13-17). Given the key role of immune system in the spleen (18-21), the spleen may play a role in psoriasis-like skin inflammation of IMQ-treated mice by modulating the immune system. However, how the spleen and splenectomy contribute to the psoriasis-like phenotype of IMQ-treated mice is unknown.

The present study investigated how the spleen impacts the psoriasis-like phenotype of IMQ-treated mice. First, we analyzed the cellular composition in the spleen of control and IMQ-treated mice by using flow cytometry. Then we examined correlations between spleen weight and cellular composition in the spleen. Second, we performed non-targeted metabolome analysis of blood samples from the two groups and examined correlations between spleen weight and blood metabolites. Finally, we determined whether splenectomy could affect psoriasis-like phenotype and skin inflammation in IMQ-treated mice.

Results

Effects of IMQ on weight and cell populations of spleen

Topical application of IMQ caused significantly increased spleen weight in IMQ-treated mice compared to control mice (**Figure 1A and 1B**), consistent with our previous report

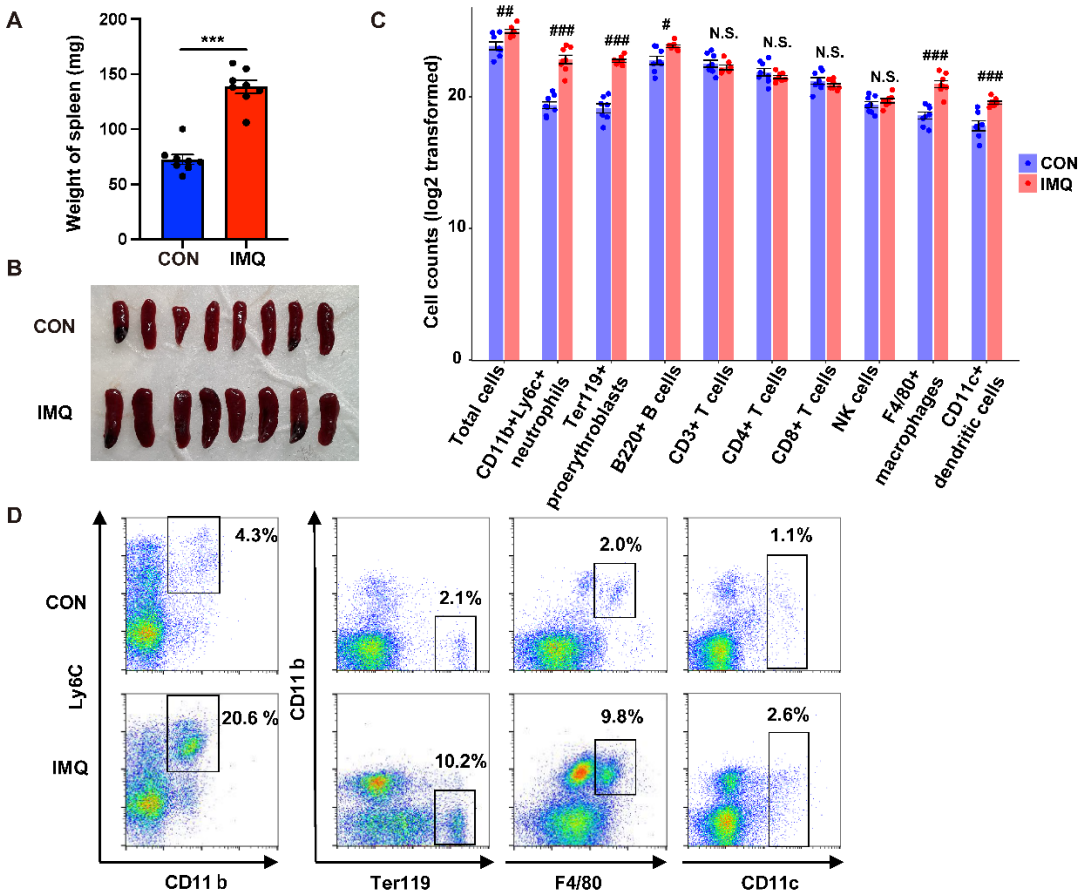

Figure 1. Effects of IMQ on weight and cell populations of spleen

(A): Spleen weight (Student t-test: df = 14, t = -9.017, P = 0.000). (B): The photos of spleen from the control group and IMQ group. (C): FACS analysis of spleen samples from the two groups. Log2 transformed data of the number of total cells and each cell type. Total cells (Mann- Whitney test: U = 7, FDR-corrected P = 0.0079), $CD11b^{+}Ly6c^{+}$ neutrophils (Mann- Whitney test: U = 0, FDR-corrected P = 0.0005), $Ter119^{+}$ proerythroblasts (Mann- Whitney test: U = 0, FDR-corrected P = 0.0006), $B220^{+}$ B cells (Mann- Whitney test: U = 8, FDR-corrected P = 0.0105), $CD3^{+}$ T cells (Mann- Whitney test: U = 19, FDR-corrected P = 0.2073), $CD4^{+}$ T cells (Mann- Whitney test: U = 22, FDR-corrected P = 0.2073), $CD8^{+}$ T cells (Mann- Whitney test: U = 19, FDR-corrected P = 0.1605), $N.K1.1^{+}$ NK cells (Mann- Whitney test: U = 22.5, FDR-corrected P = 0.2073), $F4/80^{+}$ macrophages (Mann- Whitney test: U = 0, FDR-corrected P = 0.0005), $CD11c^{+}$ DCs (Mann- Whitney test: U = 1, FDR-corrected P = 0.0009). Data are shown as mean ± SEM (n = 8). One data of $Ter119^{+}$ proerythroblasts and $CD11c^{+}$ DCs in the control group and one data of $CD3^{+}$ T cells in the IMQ group were missing because of technical problems. $^{\#}$P (FDR-corrected) < 0.05, $^{\#\#}$P (FDR-corrected) < 0.01, $^{\#\#\#}$P (FDR-corrected) < 0.001. NS: not significant. (D): The representative FACS data of $CD11b^{+}Ly6c^{+}$ neutrophils, $Ter119^{+}$proerythroblasts, $F4/80^{+}$ macrophages, and $CD11c^{+}$ DCs in the spleen of control mice and IMQ-treated mice.

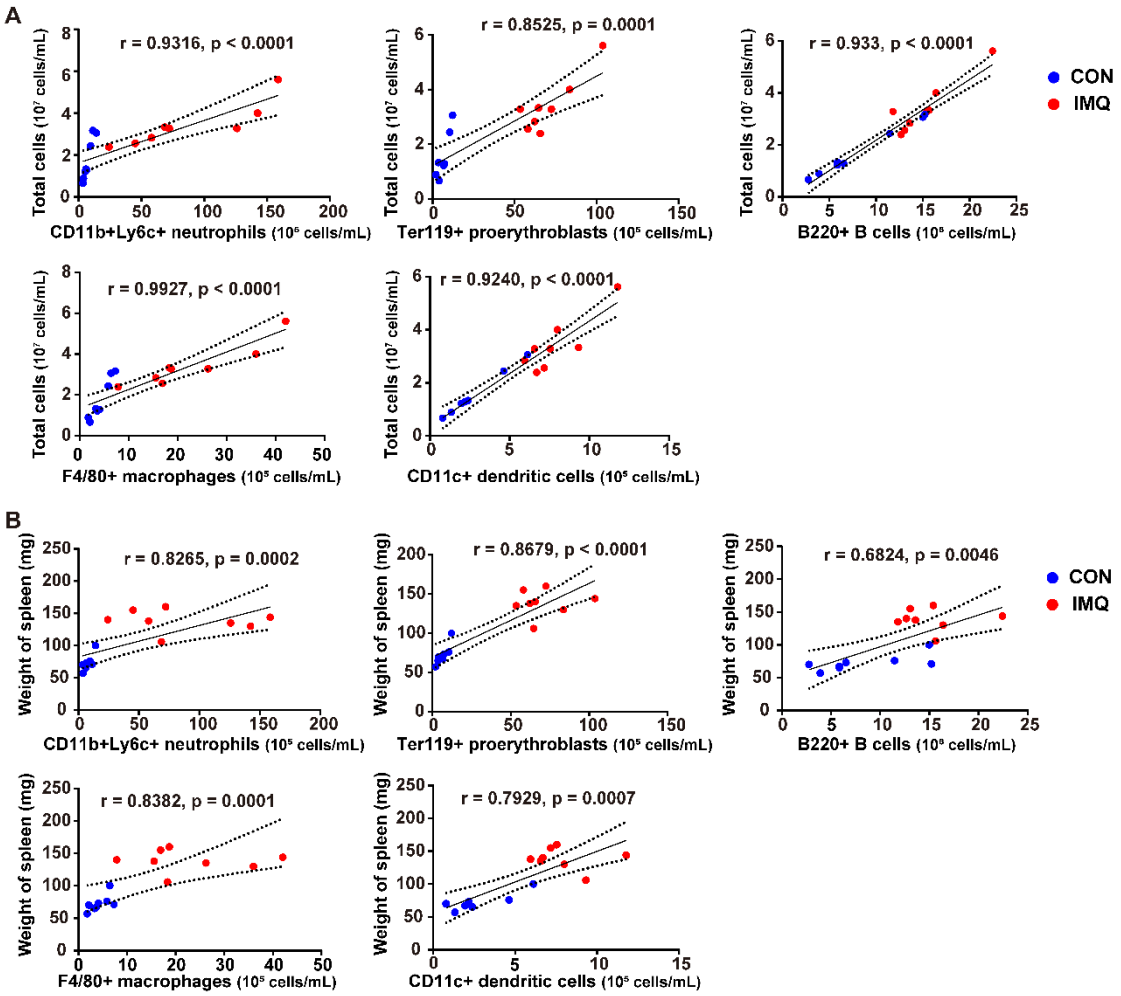

Figure 2. Correlations between the number of total splenic cells (or spleen weight) and the number of the splenic cell types

(A): The correlations between the number of total splenic cells and the number of the splenic cell types whose amount significantly increased in IMQ group. (B): The correlations between the weight of spleen and the number of the splenic cell types whose amount significantly increased in IMQ group. The values represent the mean ± SEM (n = 8).

(22). The number of total cells of IMQ-treated mice was also significantly higher than those of control mice (**Figure 1C**). Spleen cells were analyzed for the percentage and the number of $CD11b^{+}Ly6c^{+}$ neutrophils, $Ter119^{+}$ proerythroblasts, $B220^{+}$ B cells, $CD3^{+}$T cells, $CD4^{+}$ T cells, $CD8^{+}$ T cells, $NK1.1^{+}$ natural killer (NK) cells, $F4/80^{+}$ macrophages, and $CD11c^{+}$ dendritic cells (DCs). The number of neutrophils, proerythroblasts, B cells, macrophages, and DCs in the spleen of IMQ-treated mice was significantly higher than

those of control mice (**Figure 1C and 1D**). In contrast, there were no differences in the number of T cells ($CD3^+$, $CD4^+$, and $CD8^+$) and NK cells (**Figure 1C**).

The total number of cells in the spleen positively correlated with the cell types (i.e., neutrophils, proerythroblasts, B cells, macrophages, and DCs) in the two groups (**Figure 2A**). Moreover, the weight of spleen positively correlated with the cell types (i.e., neutrophils, proerythroblasts, B cells, macrophages, and DCs) in the two groups (**Figure 2B**).

Non-targeted metabolomic profiling of plasma

We performed non-targeted metabolomic profiling of plasma samples from IMQ-treated mice and control mice. After quality control and removal of low-abundance peaks, a subset of 173 metabolites was annotated. Orthogonal partial least squares discriminant analysis (OPLS-DA) revealed that the metabolic composition of IMQ group was significantly different from that of the control group (**Figure 3A**). After thresholding (variable importance in the projection [VIP] value > 0.6, Wilcoxon rank p-value < 0.05), we identified 14 metabolites altered between the two groups (**Figure 3B**). Among the 14 metabolites, taurine and 2,6-dihydroxybenzoic acid had VIP > 1.0 (**Figure 3C**). The fourteen metabolites that increased in the IMQ group were taurine, 2,6-dihydroxybenzoic acid, L-phenylalanine, 9-hydroxy-10E,12Z-octadecadienoic acid, decyl acetate, DL-malic acid, catechol, *N*-methylhydantoin, L-proline, propynoic acid, 3-ureidopropionic acid, *N,N,N*-trimethyl-lysine, L-cysteine-glutathione disulfide, and acetic acid (**Figure 3D**).

Associations between spleen cells, spleen weight, and plasma metabolites

Spearman correlation analysis was used to quantify the correlations between the spleen cell types, spleen weight, and the fourteen differential metabolites of plasma. Several cell types and spleen weight were significantly correlated with the plasma metabolites in the two groups (**Figure 4A**). The cell types such as total cells, neutrophils, and macrophages were positively associated with plasma metabolites except *N,N,N*-trimethyl-lysine. The other cell types (B cells, proerythroblasts, and DCs) were positively associated with several metabolites. Spleen weight was also positively associated with plasma metabolites except *N,N,N*-trimethyl-lysine (**Figure 4A**).

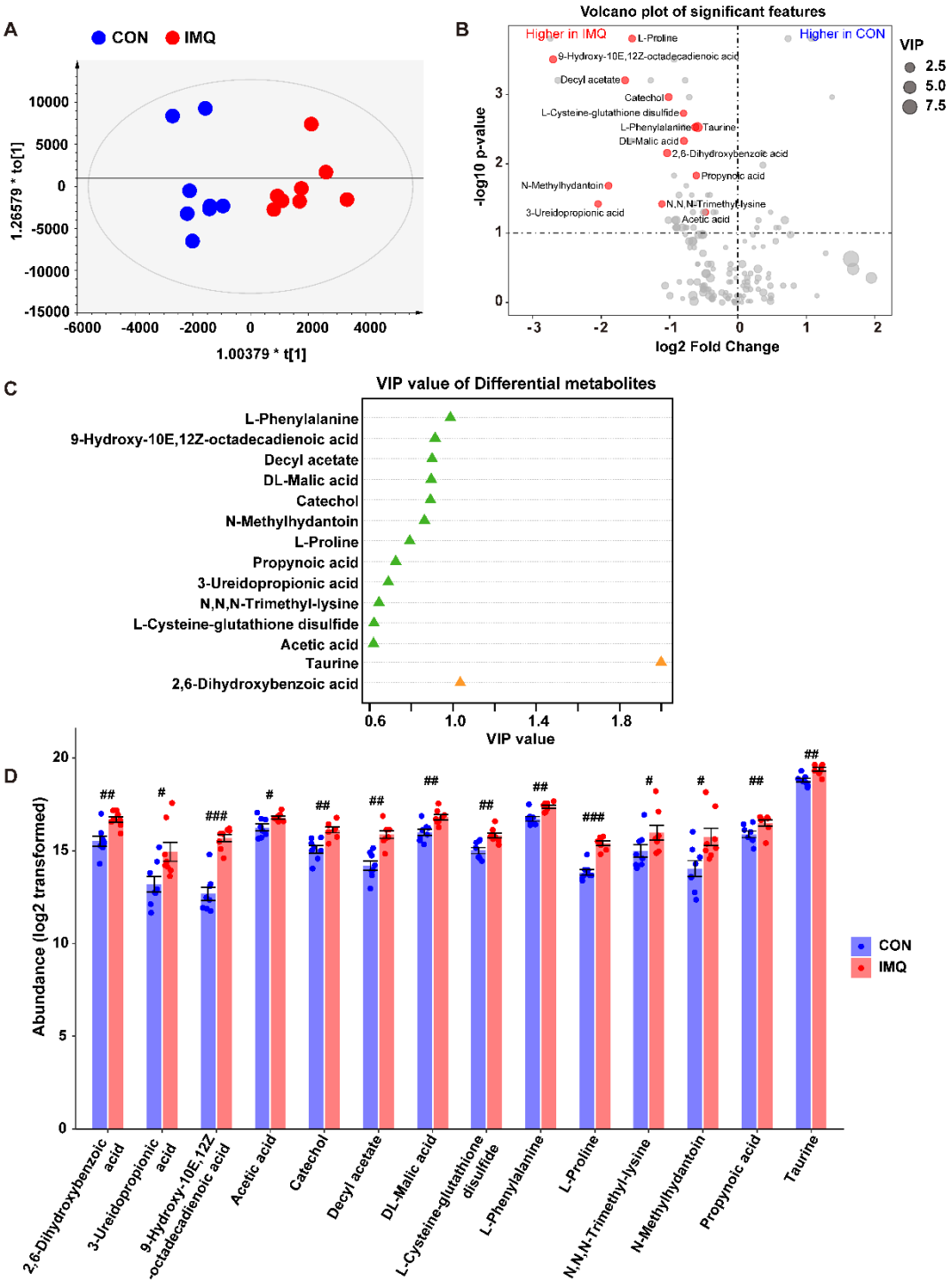
A
CON
IMQ
1.26579 * to[1]
1.00379 * t[1]
B
Volcano plot of significant features
Higher in IMQ
Higher in CON
L-Proline
9-Hydroxy-10E,12Z-octadecadienoic acid
Decyl acetate
Catechol
L-Cysteine-glutathione disulfide
L-Phenylalanine
Taurine
DL-Malic acid
2,6-Dihydroxybenzoic acid
Propynoic acid
N-Methylhydantoin
N,N,N-Trimethyllysine
3-Ureidopropionic acid
Acetic acid
VIP
2.5
5.0
7.5
-log10 p-value
log2 Fold Change
C
VIP value of Differential metabolites
L-Phenylalanine
9-Hydroxy-10E,12Z-octadecadienoic acid
Decyl acetate
DL-Malic acid
Catechol
N-Methylhydantoin
L-Proline
Propynoic acid
3-Ureidopropionic acid
N,N,N-Trimethyl-lysine
L-Cysteine-glutathione disulfide
Acetic acid
Taurine
2,6-Dihydroxybenzoic acid
VIP value
D
Abundance (log2 transformed)
CON
IMQ
2,6-Dihydroxybenzoic acid
3-Ureidopropionic acid
9-Hydroxy-10E,12Z-octadecadienoic acid
Acetic acid
Catechol
Decyl acetate
DL-Malic acid
L-Cysteine-glutathione disulfide
L-Phenylalanine
L-Proline
N,N,N-Trimethyl-lysine
N-Methylhydantoin
Propynoic acid
Taurine

Figure 3. Effects of IMQ on metabolites of plasma

(A): Scatter plot of murine plasma metabolites based on orthogonal partial least square discriminant analysis (OPLS-DA) between IMQ group and control group. (B): Volcano plot shows the differential metabolites between the two groups. The X-axis indicates the log2-transformed plasma metabolite abundance of fold change, and the Y-axis indicates the -log10-transformed P value using the Wilcoxon rank sum test. Horizontal lines indicate $P < 0.05$. Increased or decreased metabolites are marked in red and blue, respectively. The size of the dot represents the size of the VIP value. Metabolites with $P < 0.05$ and VIP > 0.6 are mentioned in text. (C): VIP value of the differential metabolites between the two groups. (D): Log2 transformed data of the abundance of the differential plasma metabolites. 2,6-dihydroxybenzoic acid (Mann- Whitney test: U = 7, FDR-corrected P = 0.0047), 3-ureidopropionic acid (Mann- Whitney test: U = 12, FDR-corrected P = 0.0177), 9-hydroxy-10E,12Z-octadecadienoic acid (Mann- Whitney test: U = 1, FDR-corrected P = 0.0009), acetic acid (Mann- Whitney test: U = 13, FDR-corrected P = 0.0216), catechol (Mann- Whitney test: U = 3, FDR-corrected P = 0.0016), decyl acetate (Mann- Whitney test: U = 2, FDR-corrected P = 0.0013), DL-malic acid (Mann- Whitney test: U = 6, FDR-corrected P = 0.0035), L-cysteine-glutathione disulfide (Mann- Whitney test: U = 4, FDR-corrected P = 0.0023), L-phenylalanine (Mann- Whitney test: U = 5, FDR-corrected P = 0.0026), L-proline (Mann- Whitney test: U = 0, FDR-corrected P = 0.0009), *N,N,N*-trimethyl-lysine (Mann-Whitney test: U = 12, FDR-corrected P = 0.0177), *N*-methylhydantoin (Mann- Whitney test: U = 10, FDR-corrected P = 0.0114), propynoic acid (Mann- Whitney test: U = 9, FDR-corrected P = 0.0089), taurine (Mann- Whitney test: U = 5, FDR-corrected P = 0.0026). Data are shown as mean ± SEM (n = 8). $^{\#}$P (FDR-corrected) < 0.05, $^{\#\#}$P (FDR-corrected) < 0.01, $^{\#\#\#}$P (FDR-corrected) < 0.001.

Spearman correlation was also used to determine if IMQ-related cell types in the spleen and plasma metabolites contribute to splenomegaly. The cell types in the spleen and plasma metabolites differentially abundant in the two groups showed more associations with spleen weight (**Figure 4B**). Interestingly, neutrophils in the spleen were positively correlated with spleen weight and plasma metabolites (**Figure 4B**).

Effect of splenectomy on skin inflammation and body weight changes in IMQ-treated mice

Topical application of IMQ induced psoriasis-like dermatitis in both sham group and splenectomy group (**Figure 5A)**. Representative hematoxylin and eosin staining of the back skin showed acanthosis and parakeratosis with microabscess in the two groups

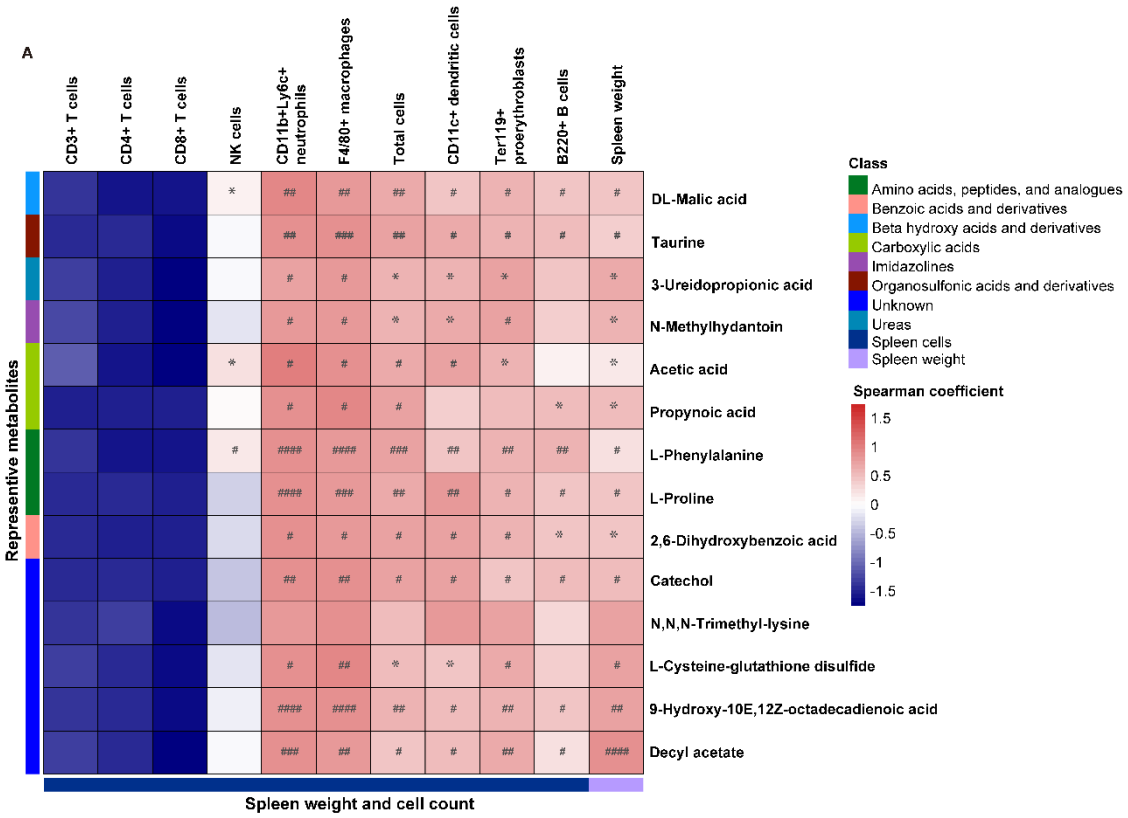
A
CD3+ T cells
CD4+ T cells
CD8+ T cells
NK cells
CD11b+Ly6c+ neutrophils
F4/80+ macrophages
Total cells
CD11c+ dendritic cells
Ter119+ proerythroblasts
B220+ B cells
Spleen weight
DL-Malic acid
Taurine
3-Ureidopropionic acid
N-Methylhydantoin
Acetic acid
Propynoic acid
L-Phenylalanine
L-Proline
2,6-Dihydroxybenzoic acid
Catechol
N,N,N-Trimethyl-lysine
L-Cysteine-glutathione disulfide
9-Hydroxy-10E,12Z-octadecadienoic acid
Decyl acetate
Representive metabolites
Spleen weight and cell count
Class
Amino acids, peptides, and analogues
Benzoic acids and derivatives
Beta hydroxy acids and derivatives
Carboxylic acids
Imidazolines
Organosulfonic acids and derivatives
Unknown
Ureas
Spleen cells
Spleen weight
Spearman coefficient
1.5
1
0.5
0
-0.5
-1
-1.5
B
CD8+ T cells
CD4+ T cells
CD3+ T cells
NK cells
Spleen weight
Ter119+ proerythroblasts
9-Hydroxy-10E,12Z-octadecadienoic acid
F4/80+ macrophages
Decyl acetate
B220+ B cells
L-Phenylalanine
CD11b+Ly6c+ neutrophils
DL-Malic acid
CD11c+ dendritic cells
Total cells
L-Proline
3-Ureidopropionic acid
Catechol
2,6-Dihydroxybenzoic acid
Taurine
L-Cysteine-glutathione disulfide
N-Methylhydantoin
N,N,N-Trimethyl-lysine
Propynoic acid
Node shape
Spleen cells
Spleen weight
Metabolite
Relation
Positive
Spearman coefficient
0.70
0.99

Figure 4. Associations among spleen cell types, spleen weight and the metabolites of plasma samples

(A): Heatmap of Spearman rank correlation coefficients between counts of splenic cell types or spleen weight and the metabolites of plasma samples. $^{*}P < 0.05$ and FDR-corrected $P > 0.05$, $^{\#}P$ (FDR-corrected) < 0.05, $^{\#\#}P$ (FDR-corrected) < 0.01, $^{\#\#\#}P$ (FDR-corrected) < 0.001, $^{\#\#\#\#}P$ (FDR-corrected) < 0.0001. (B): Correlation network analysis reveals the associations among counts of spleen cell types, spleen weight and the plasma metabolites. Each node shape represents spleen cell types, spleen weight or plasma metabolites, respectively. The pink lines connecting the nodes indicate positive correlation and the line weight indicates spearman correlation coefficient. We created the network using Cytoscape software 3.8.0. (https:cytoscape.org).

(**Figure. 5B**). The cumulative scores of the sham-IMQ group and splenectomy-IMQ group were not significantly different (**Figure 5C**).

Next, we measured the gene expression levels of IL-17A and IL-23A in the skin. The mRNA levels of IL-17A and IL-23A in the IMQ group were higher than those of the control group (**Figure 5D**). Expression of IL-17A mRNA in the splenectomy-IMQ group was significantly higher than that of sham-IMQ group, whereas the expression of IL-23A mRNA was not different between the sham-IMQ group and splenectomy-IMQ group (**Figure 5D**). There were also no changes in the body weight between sham group and splenectomy group in both of IMQ group and control group (**Figure 5E**).

Discussion

This is the first study to show how the spleen contributes to psoriasis-like phenotypes in IMQ-treated mice. Indeed, topical application of IMQ significantly increased infiltration of immune cells such as neutrophils, DCs, macrophages, and B cells in the spleen, which agrees with previous studies. These cell types correlated with spleen weight, which also correlated with higher levels of 14 metabolites in the plasma of IMQ-treated mice; taurine and 2,6-dihydroxybenzoic acid had especially high VIP values. These metabolites likely contribute to splenomegaly upon IMQ application. Finally, we showed that splenectomy does not affect a psoriasis-like phenotype on the skin of IMQ-treated mice but could potentiate IMQ-induced increases in IL-17A mRNA in the skin.

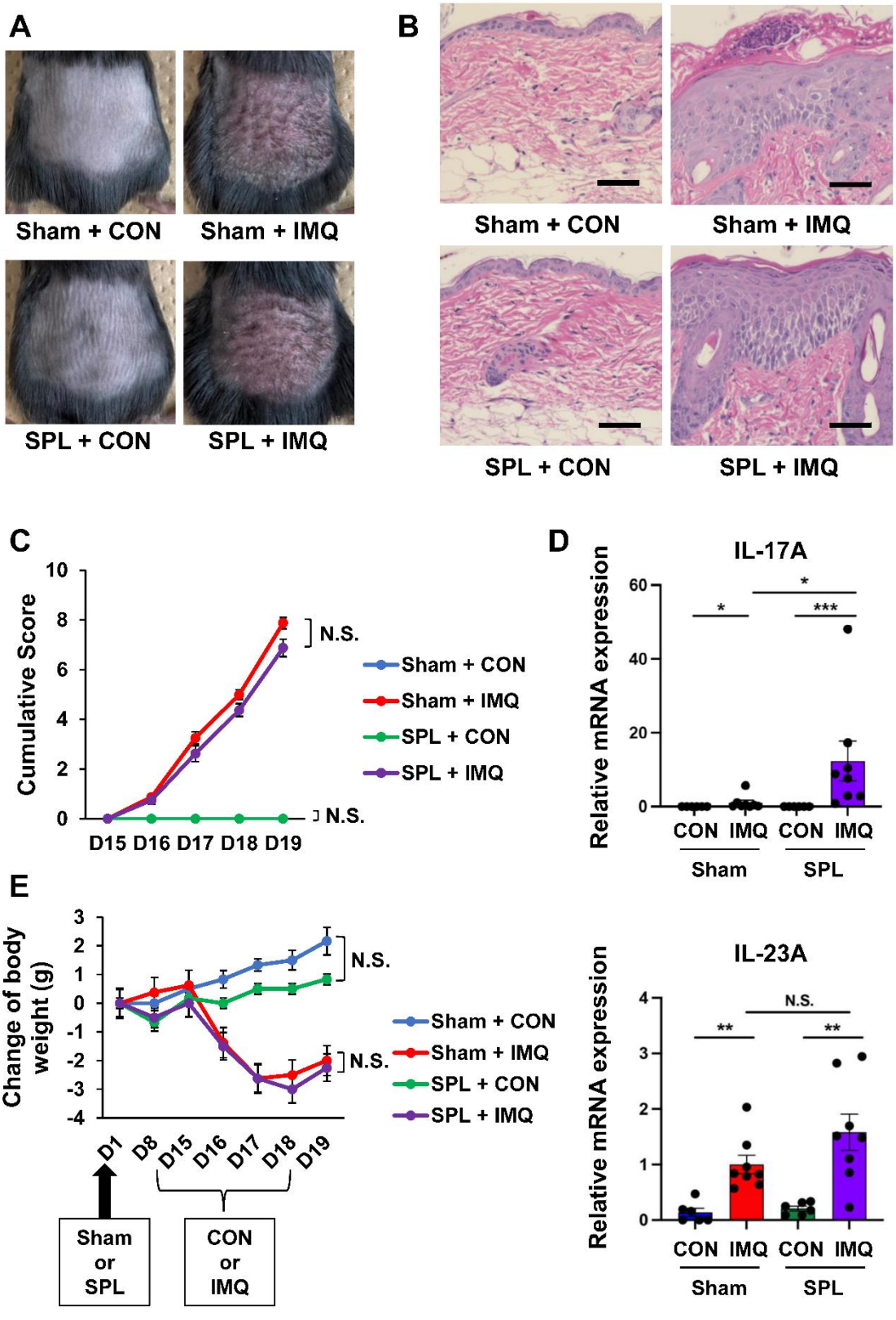
A
Sham + CON
Sham + IMQ
SPL + CON
SPL + IMQ
B
Sham + CON
Sham + IMQ
SPL + CON
SPL + IMQ
C
Cumulative Score
10
8
6
4
2
0
N.S.
N.S.
D15 D16 D17 D18 D19
Sham + CON
Sham + IMQ
SPL + CON
SPL + IMQ
D
IL-17A
Relative mRNA expression
60
40
20
0
*
*
***
CON IMQ CON IMQ
Sham
SPL
E
Change of body weight (g)
3
2
1
0
-1
-2
-3
-4
N.S.
N.S.
D1 D8 D15 D16 D17 D18 D19
Sham or SPL
CON or IMQ
Sham + CON
Sham + IMQ
SPL + CON
SPL + IMQ
IL-23A
Relative mRNA expression
4
3
2
1
0
N.S.
**
**
CON IMQ CON IMQ
Sham
SPL

Figure 5. Effect of splenectomy on the skin inflammation and body weight changes in IMQ-treated mice

(A): Mice were treated topically with 5% IMQ cream or control cream on the shaved back for four days two weeks after sham or splenectomy. The representative photos of back skin from the four groups. (B): HE staining of the back skin. Scale bar = 50 μm. (C): Cumulative skin scores from day 15 to day 19. Day 15 (Kruskal-Wallis test: H = 0.000, P = 1.000), day 16 (Kruskal-Wallis test: H = 17.792, P = 0.000), day 17 (Kruskal-Wallis test: H = 22.840, P = 0.000), day 18 (Kruskal-Wallis test: H = 23.619, P = 0.000), day 19 (Kruskal-Wallis test: H = 23.459, P = 0.000). Scores of sham + control group and splenectomy + control group are 0 from D15 to D19. (D): Relative mRNA expression levels of IL-17A and IL23-A in murine back skin. IL-17A mRNA (Kruskal-Wallis test: H = 23.332, P = 0.000), IL-23A mRNA (Kruskal-Wallis test: H = 19.302, P = 0.000). *P <0.05, **P <0.01, ***P <0.001. (E): Change of body weight. Day 1 (Kruskal-Wallis test: H = 0.000, P = 1.000), day 8 (Kruskal-Wallis test: H = 7.641, P = 0.054), day 15 (Kruskal-Wallis test: H = 2.022, P = 0.568), day 16 (Kruskal-Wallis test: H = 10.921, P = 0.012), day 17 (Kruskal-Wallis test: H = 20.213, P = 0.000), day 18 (Kruskal-Wallis test: H = 21.758, P = 0.000), day 19 (Kruskal-Wallis test: H = 20.287, P = 0.000). The values represent the mean ± SEM. (n = 6 or 8). NS: not significant. SPL: Splenectomy.

Neutrophils, proerythroblasts, B cells, macrophages, and DCs significantly enlarged the IMQ-treated spleen; their cell compartments positively correlated with spleen weight. Interestingly, the percentage of B cells in the spleen did not change between the control group and IMQ-treated group. Previously, percentages of macrophages and DCs increased and the percentage of T cells (both $CD4^{+}$ and $CD8^{+}$) decreased in an IMQ-treated group (9), consistent with the current data. Topical treatment with IMQ likely induces inflammation, and increased numbers of immune cells cause splenomegaly.

The longitudinal diameter of the spleen and the duration of psoriasis were correlated in a previous study of 79 psoriatic patients (23), suggesting that increased diameter of the spleen in psoriatic patients with long-term illness is related to chronic inflammation. Future clinical studies are needed to confirm the role of spleen in the pathogenesis of psoriasis (24).

Non-targeted metabolomics profiling identified 14 metabolites whose levels were significantly different between the IMQ-treated group and the control group. Taurine and 2,6-dihydroxybenzoic acid had the highest VIP values, indicating that they

contributed the most to the separation between groups. Taurine plays an important role in inflammation associated with oxidative stress (25,26) and may play a pathological role in psoriasis given its higher levels in blood from patients with psoriasis when compared to healthy controls (27). Taurine reduced blood levels of IL-6 in patients with traumatic brain injury in a recent randomized double-blind controlled trial (28). Taurine's anti-inflammatory actions (25,26) in the blood of IMQ-treated mice may compensate for IMQ-induced inflammation in the body. Further studies should explore how taurine affects spleen size in IMQ-treated mice. The function of 2,6-dihydroxybenzoic acid remains unclear but is likely anti-inflammatory (29). Higher levels of 2,6-dihydroxybenzoic acid in the blood of IMQ-treated mice may also compensate for IMQ-induced inflammation in the body. These metabolites should be targeted in future studies on splenomegaly of IMQ-treated mice.

Spleen enlargement is linked to systemic inflammation (30). For example, we reported splenomegaly in mice treated with lipopolysaccharide (LPS), and there were positive correlations between spleen weight and blood levels of pro-inflammatory cytokines (i.e., IL-6, tumor necrosis factor-α) (31-33). A chronic social defeat stress (CSDS) model revealed that the spleen weight of susceptible mice with depression-like behaviors was higher than that of control mice and CSDS-resilient mice (34). Collectively, it is likely that LPS- (or CSDS)-induced splenomegaly is associated with systemic inflammation (31-36).

Considering the spleen's key role in the immune system (18-21), we investigated how splenectomy affects psoriasis-like pathology and skin inflammation of IMQ-treated mice. Unexpectedly, splenectomy did not change the psoriasis-like phenotype in IMQ-treated mice. However, we found that splenectomy significantly enhanced IL-17A mRNA in the skin of IMQ-treated mice compared to sham-operated mice. The spleen may not directly impact the psoriasis-like phenotype of IMQ-treated mice, but it does cause splenomegaly.

This study has one limitation. In this study, we used 5% IMQ cream (Beselna cream). The full list of excipients is isostearic acid, benzyl alcohol, cetyl alcohol, stearyl alcohol, white soft paraffin, polysorbate 60, sorbitan stearate, glycerol, methyl hydroxybenzoate, propyl hydroxybenzoate, xanthan gum, and purified water. Walter et

al. (37) reported that isostearic acid, a major component, could promote inflammasome activation in cultured keratinocytes, and that it increased the expression of inflammatory cytokines *in vivo*. These data suggest that isostearic acid may contribute to the observed effects of Beselna cream used in this study (37,38). In this study, we did not examine the effects of isosteatic acid on spleen function since the company did not disclose the detailed information of excipients including isostearic acid. Further study is needed to investigate the effects of isostearic acid on spleen functions.

In conclusion, this study highlighted the key role of the spleen in chronic inflammation of IMQ-treated mice. The numbers of neutrophils, proerythroblasts, B cells, macrophages, and DCs in the spleen significantly increased, which correlated with higher spleen weight. Metabolomics profiling also revealed metabolites whose roles in psoriasis pathogenesis can be studied further. However, splenectomy did not affect psoriasis-like phenotypes in IMQ-treated mice. Although the spleen may not play a major role in psoriasis-like phenotypes in IMQ-treated mice, topical application of IMQ to back skin causes splenomegaly.

Materials and Methods

Animals

Nine-week-old female C57BL/6 mice (weighing 18–21 g, n = 16, Japan SLC Inc., Hamamatsu, Shizuoka, Japan) were used in Experiment 1. Seven-week-old female C57BL/6 mice (weighing 18–21 g, n = 28, Japan SLC Inc., Hamamatsu, Shizuoka, Japan) were used in Experiment 2. Mice were housed (3–4 per cage) under a 12-h/12-h light/dark cycle (lights on between 07:00 and 19:00), with *ad libitum* access to food (CE-2; CLEA Japan, Inc., Tokyo, Japan) and water. The experimental protocol was approved by the Chiba University Institutional Animal Care and Use Committee (Permission number: 2-433). All procedures were performed in accordance with the relevant guidelines and regulations, and the study complied with ARRIVE (Animal Research: Reporting of In Vivo Experiments) guidelines. All efforts were made to minimize animal suffering (22).

IMQ treatment

The shaved back skin of mice was treated with 62.5 mg of 5% IMQ cream (Beselna

cream; Mochida Pharmaceutical Co., Tokyo, Japan) daily for four consecutive days as previously described (22). Control mice were treated similarly with 62.5 mg of white petrolatum (Maruishi Pharmaceutical Co., Osaka, Japan).

Splenectomy

Splenectomy (or sham) surgery was performed under continuous isoflurane inhalation anesthesia as previously described (39). Briefly, the mice were anesthetized with 3% isoflurane through an inhalation anesthesia apparatus (KN-1071NARCOBIT-E; Natsume Seisakusho, Tokyo, Japan). In the splenectomy group, each mouse was maintained in a right lateral recumbent position, and an approximately 1-cm incision was made from the abdominal wall under the left costal margin. The skin was dissected, and subcutaneous, muscle, and fascia layers were removed individually until the spleen was exposed. The peripheral ligament of the spleen was separated, associated blood vessels and nerves were ligatured using 6-0 silk sutures, and the spleen was removed by transecting the blood vessels distal to the ligature. Abdominal muscles and the skin incision were closed sequentially using 4-0 silk sutures. The abdominal wall was similarly opened during sham surgery, and the wall was closed immediately after identifying the spleen (39). In this study, we did not use opioid and/or non-steroidal anti-inflammatory drugs for pain management after surgery.

Sample collection

Experiment 1: After IMQ treatment for four consecutive days, the skin, spleen, and blood samples were collected on day 5.

Experiment 2: Splenectomy or sham was carried out on day 1. Mice were treated with IMQ from day 15 to day 18, and skin samples were collected on day 19. The clinical skin score was measured from day 15 to day 19. The degree of skin inflammation was assessed with a cumulative disease severity score, similar to the human Psoriasis Area and Severity Index but without considering the area. Erythema, scaling, and thickening were scored independently from 0 to 4: 0, none; 1, slight; 2, moderate; 3, marked; 4, very marked. The single scores were summed; the highest possible score is 12 (9).

Fluorescence activated cell sorting analysis of spleen samples

Mouse spleen tissues were mashed and passed through a 100-μm mesh to prepare a single cell suspension and treated with lysis buffer (0.155 M ammonium chloride, 0.1M

disodium EDTA, 0.01M potassium bicarbonate) to lyse erythrocytes. Spleen cells were suspended and counted using an automated cell counter (BIO-RAD, Alfred Nobel Drive, CA) prior to fluorescence activated cell sorting (FACS) analysis. We stained 10^6 cells with various monoclonal antibodies against cell surface antigens for 30 min at 4 °C and then washed them with an FACS buffer [3% fetal calf serum (FCS), 0.04% NaN3 in phosphate-buffered saline]. Cells were resuspended with 0.4 μg/ml propidium iodine (cat# P-170: Sigma) containing FACS buffer. The following antibodies were used: anti CD11b-PE (×400 diluted using FACS buffer, cat# 553312: BD Bioscience, Franklin Lakes, NJ), anti Ly6c-FITC (×100, cat# 553104: BD Bioscience), anti B220-PE (×200, cat# 553309: BD Bioscience), anti CD8alpha-allophycocyanin (×100, cat# 553035: BD Bioscience), anti NK1.1-PE (×100, cat# 553165: BD Bioscience), anti CD11c-PE (×100, cat# 557401: BD Bioscience), anti Ter119-PE (×40, cat# 12-5921-83: eBioscience, San Diego, CA), anti CD4-allophycocyanin (×100, cat# 17-0042-82: eBioscience, San Diego, CA), anti F4/80-PE (×40, cat# 12-4801-80: Invitrogen), and anti CD3-FITC (×40, cat# 100305: BioLegend, San Diego, CA). The stained cells were analyzed using FACSCantII and FlowJo software (BD Bioscience).

Untargeted metabolomics analysis of plasma samples

Untargeted metabolomics analysis was performed using an ExionLC AD UPLC system (SCIEX, Tokyo, Japan) interfaced with an X500R LC-QToFMS system (SCIEX, Tokyo, Japan) with electrospray ionization (ESI) operating in positive and negative ionization mode, as previous reported (40,41). First, 100 μL of methanol containing internal standards (100 μM *N,N*-diethyl-2-phenylacetamide and d-camphor-10-sulfonic acid) was added to the plasma samples (100 μL), and then samples were centrifuged at 14,000 × rpm for 5 min. After centrifugation, the supernatant was transferred to an Amicon® Ultra-0.5 3 kDa filter column (Merck Millipore, Tokyo, Japan) and centrifuged at 14,000 × rpm for 1 h. The filtrate was transferred to glass vials for subsequent analysis.

The metabolomics data was analyzed with Mass Spectrometry-Data Independent AnaLysis (MS-DIAL) software version 4.60 (42) and R statistical environment Ver 4.0.5. Only metabolites present in 50% of the samples were measured, and metabolites whose coefficient of variation value was over 30% in pooled QC samples were removed from analysis. Annotation level 2 proposed by Schymanski et al. (43) was used for data

analysis.

Histology

Back skin samples from control and IMQ-treated groups were collected and fixed in 10% formalin (FUJIFILM Wako Pure Chemical Corp., Tokyo, Japan). Staining with hematoxylin and eosin (HE) was performed at the Biopathology Institute Co., Ltd (Kunisaki, Oita, Japan) as previously reported (22). Back skin samples were embedded in paraffin, and 3-μm sections were prepared and stained with HE. Representative images of two groups were obtained using a Keyence BZ-9000 Generation II microscope (Osaka, Japan) as previously reported (22).

Quantitative real-time polymerase chain reaction

RNA was isolated using TRIzol LS Reagent (Invitrogen, Carlsbad, CA, USA) according to the manufacturer's instructions; cDNA was generated using the High-Capacity cDNA Reverse Transcription Kit (Applied Biosystems, Waltham, MA, USA) and TaKaRa polymerase chain reaction (PCR) Thermal Cycler Dice (Takara Bio Inc., Kusatsu, Shiga, Japan), and quantitative real-time PCR was performed using the StepOnePlus Real-Time PCR System (Applied Biosystems, Waltham, MA, USA). The mouse primers for glyceraldehyde-3-phosphate dehydrogenase (GAPDH) (4352339E), IL-17A (Mm00439618), and IL-23A (Mm00518984) were obtained from Applied Biosystems. The GAPDH housekeeping gene was used to normalize gene expression.

Statistical analysis

Data are shown as the mean ± standard error of the mean. Data were analyzed using GraphPad Prism (Tokyo, Japan). Student's t-test was performed to compare spleen weights between the two groups. Spleen cell types and plasma metabolites were compared between the two groups using Mann-Whitney U-test with a false discovery rate (FDR) control. Correlations among spleen weight, spleen cells, and plasma metabolites were evaluated using Spearman's correlation analysis. For multivariate analysis of the metabolome data, orthogonal partial least squares discriminant analysis (OPLS-DA) was performed in Simca-P V.14.0 (Umetrics AB). Metabolites with VIP > 0.6 and p-value < 0.05 (Wilcoxon rank-sum test) were considered differentially abundant. Cumulative skin score, relative mRNA expression of skin, and body weight

changes were analyzed with a Kruskal–Wallis test. $P < 0.05$ (or FDR-corrected $P < 0.05$) was considered statistically significant.

References

1. Mease, P.J. et al. Prevalence of rheumatologist – diagnosed psoriatic arthritis in patients with psoriasis in European/North American dermatology clinics. *J. Am. Acad. Dermatol.* **59,** 729-735 (2013). doi: 10.1016/j.jaad.2013.07.023.
2. Ghoreschi, K., Balato, A., Enerbäck, C. & Sabat, R. Therapeutic targerting the IL-23 and IL-17 pathway in psoriasis. *Lancet* **397,** 754-766 (2021). doi: 10.1016/S0140-6736(21)00184-7.
3. Griffiths, C.E.M., Armstrong, A.W., Gudjonsson, J.E. & Barker, J.N.W.N. Psoriasis. *Lancet* **397,** 1301-1315 (2021). doi: 10.1016/S0140-6736(20)32549-6.
4. Sharma, A. *et al*. IL-23/Th17 axis: a potential therapeutic tagrget for psoriasis. *Curr. Drug Res. Rev.* **14,** 24-36 (2022). doi: 10.2174/2589977513666210707114520.
5. Nestle, F.O., Kaplan, D.H. & Barker, J. Psoriasis. *N. Engl. J. Med.* **361**, 496-509 (2009). doi: 10.1056/NEJMra0804595.
6. Boehncke, W.H. & Schön, M.P. Psoriasis. *Lancet* **386**, 983-994 (2015). doi: 10.1016/S0140-6736(14)61909-7.
7. Rendon, A. & Schäkel, K. Psoriasis pathogenesis and treatment. *Int. J. Mol. Sci.* **20,** 1475 (2019). doi: 10.3390/ijms20061475.
8. Armstrong, A.W. & Read, C. Pathophysiology, clinical presentation, and treatment of psoriasis: a review. *JAMA* **323**, 1945-1960 (2020). doi: 10.1001/jama.2020.4006.
9. van der Fits, L. *et al*. Imiquimod-induced psoriasis-like skin inflammation in mice is mediated via the IL-23/IL-17 axis**.** *J. Immunol.* **182**, 5836-5845 (2009). doi: 10.4049/jimmunol.0802999.
10. Flutter, B. & Nestle, F.O. TLRs to cytokines: Mechanistic insights from the imiquimod mouse model of psoriasis. *Eur. J. Immunol.* **43**, 3138-3146 (2013). doi: 10.1002/eji.201343801.
11. Slominski, A. & Wortsman, J. Neuroendocrinology of the skin. *Endocr. Rev.* **21**, 457-487 (2000). doi: 10.1210/edrv.21.5.0410.
12. Slominski, A.T., Manna, P.R. & Tuckey, R.C. On the role of skin in the regulation

of local and systemic steroidogenic activities. *Steroids* **103**, 72-88 (2015). doi: 10.1016/j.steroids.2015.04.006.

13. Qin, S. *et al*. Endogenous n-3 polyunsaturated fatty acids protect against imiquimod-induced psoriasis-like inflammation via the IL-17/IL-23 axis. *Mol. Med. Rep.* 9, 2097-2104 (2014). doi: 10.3892/mmr.2014.2136.
14. Huang, S.W. *et al.* Azithromycin impairs TLR7 signaling in dendritic cells and improves the severity of imiquimod-induced psoriasis-like skin inflammation in mice. *J. Dermatol. Sci.* **84,** 59-70 (2016). doi: 10.1016/j.jdermsci.2016.07.007.
15. Lee, J. *et al*. Tussilagonone ameliorates psoriatic fearures in keratinocytes and imiquimod-induced psoriasis-like lesions in mice via NRF2 activation. *J. Invbest. Dermatol.* **140**, 1223-1232 (2020). doi: 10.1016/j.jid.2019.12.008.
16. Schwarz, A., Philippsen, R. & Schwarz, T. Induction of regulatory T cells and correction of cytokine disbalance by short-chain fatty acids: Implications for psoriasis therapy. *J. Invest. Dermatol.* **141**, 95-104 (2021). doi: 10.1016/j.jid.2020.04.031.
17. Zhang, S. *et al.* Hyperforin ameliorates imiquimod-induced psoriasis-like murine skin inflammation by modulating IL-17A-producing gammadelta T cells. *Front. Immunol.* **12,** 635076 (2021). doi: 10.3389/fimmu.2021.635076.
18. Mebius, R.E. & Kraal, G. Structure and function of the spleen. *Nat. Rev. Immunol.* **5,** 606-616 (2005). doi: 10.1038/nri1669.
19. Bronte, V. & Pittel M.J., The spleen in local and systemic regulation of immunity. *Immunity* **39,** 806-818 (2013). doi: 10.1016/j.immuni.2013.10.010.
20. Lewis, S.M., Williams, A. & Eisenbarth, S.C. Structure and function of the immune system in the spleen. *Sci. Immunol.* **4,** eaau6085 (2019). doi: 10.1126/sciimmunol.aau6085.
21. Wei, Y. *et al*. Brain - spleen axis in health and diseases: a review and future perspective. *Brain Res. Bull.* **182,** 130-140 (2022). doi: 10.1016/j.brainresbull.2022.02.008.
22. Shinno-Hashimoto, H. *et al*. Abnormal composition of microbiota in the gut and skin of imiquimod-treated mice. *Sci. Rep.* **11,** 11265 (2021). doi: 10.1038/s41598-021-90480-4.
23. Balato, N. *et al*. Nonalcoholic fatty liver disease, spleen and psoriasis: New aspects of low-grade chronic inflammation. *Word J. Gastroenterol.* **21,** 6892-6897 (2015).

doi: 10.3748/wjg.v21.i22.6892.

24. Di, T. *et al*. Study on the effect of spleen deficiency on the pathogenesis of psoriasis based on intestinal microbiome. *Longhua Chin. Med.* **2,** 14 (2019). doi: 10.21037/lcm.2019.09.02.
25. Marcinkiewicz, J. & Kontny, E. Taurine and inflammaotory diseases. *Amino Acids* **46,** 7-20 (2014). doi: 10.1007/s00726-012-1361-4.
26. Niu, X., Zheng, S., Liu, H. & Li, S. Protective effects if taurine against inflammation, apoptosis, and oxidative stress in brain injury. *Mol. Med. Rep.* **18,** 4516-4522 (2018). doi: 10.3892/mmr.2018.9465.
27. Ottas, A. *et al*. The metabolic analysis of psoriasis identifies the associated metabolites while providing computational models for the monitoring of the disease. *Arch. Dermatol. Res.* **309,** 519-528 (2017). doi: 10.1007/s00403-017-1760-1.
28. Vahdat, M. *et al*. The effects of Taurine supplementation on inflammatory markers and clinical outcomes in patients with traumatic brain injury: a double-blind randomized controlled trial. *Nutr. J.* **20,** 53 (2021). doi: 10.1186/s12937-021-00712-6.
29. Lightowler, L.E. & Rylance, H.J. Substituted dihydroxybenzoic acids as possible anti-inflammatory agents. *J. Pham. Pharmacol.* **15,** 633-638 (1963).
30. Smith, K.G. & Hunt, J.L. On the use of spleen mass as a measure of avian immune system strengh. *Ecophysiology* **138,** 28-31 (2004). doi: 10.1007/s00442-003-1409-y.
31. Zhang, J. *et al*. A key role of the subdiaphragmatic vagus nerve in the depression-like phenotype and abnormal composition of gut microbiota in mice after lipopolysaccharide administration. *Transl. Psychiatry* **10,** 186 (2020). doi: 10.1038/s41398-020-00878-3.
32. Zhang, J. *et al*. (*R*)-Ketamine attenuates LPS-induced endotoxin-derived delirium through inhibition of neuroinflammation. *Psychopharmacology (Berl)* **238,** 2743-2753 (2021). doi: 10.1007/s00213-021-05889-6.
33. Ma, L. *et al*. Nuclear factor of activated T cells 4 in the prefrontal cortex is required for prophylactic actions of (*R*)-ketamine. *Transl. Psychiatry* **12,** 27 (2022). doi:

10.1038/s41398-022-01803-6.

34. Zhang, K. *et al.* Splenic NKG2D confers resilience versus susceptibility in mice after chronic social defeat stress: beneficial effects of (*R*)-ketamine. *Eur. Arch. Psychiatry Clin. Neurosci.* **271,** 447-456 (2021). doi: 10.1007/s00406-019-01092-z.
35. Hashimoto, K. Molecular mechanisms of the rapid-acting and long-lasting antidepressant actions of (*R*)-ketamine. *Biochem. Pharmacol.* **177,** 113935 (2020). doi: 10.1016/j.bcp.2020.113935.
36. Wei, Y., Chang, L. & Hashimoto, K. Molecular mechanisms underlying the antidepressant actions of arketamine: beyond the NMDA receptor. Mol. Psychiatry **27,** 559-573 (2022). doi: 10.1038/s41380-021-01121-1.
37. Walter, A. et al.: Aldara activates TLR7-independent immune defence. *Nat. Commun.* **4,** 1560 (2013). doi: 10.1038/ncomms2566.
38. Flutter, B. & Nestle, F.O. TLRs to cytokines: mechanistic insights from the imiquimod mouse model of psoriasis. *Eur. J. Immunol.* **43**, 3138-3146 (2013). doi: 10.1002/eji.201343801.
39. Wei, Y. *et al*. Abnormalities of the composition of the gut microbiota and short-chain fatty acids in mice after splenectomy. *Brain Beahv. Imun. Health* **11**, 100198 (2021). doi: 10.1016/j.bbih.2021.100198.
40. Wan, X. *et al.* Effects of (*R*)-ketamine on reduced bone mineral density in ovariectomized mice: A role of gut microbiota. *Neuropharmacology* 213, 109139. doi: 10.1016/j.neuropharm.2022.109139.
41. Wan, X. *et al.* Gut-microbiota-brain axis in the vulnerability to psychosis in adulthood after repeated cannabis exposure during adolescence. *Eur. Arch. Psychiatry Clin. Neurosci.* 2022 Jun 6. doi: 10.1007/s00406-022-01437-1.
42. Tsugawa, H. *et al*. MS-DIAL: data-independent MS/MS deconvolution for comprehensive metabolome analysis. *Nat. Methods* **12,** 523-526 (2015). doi: 10.1038/nmeth.3393.
43. Schymanski, E.L., *et al*. Identifying small molecules via high resolution mass spectrometry: communicating confidence. *Environ. Sci. Technol.* **48,** 2097-2098 (2014). doi: 10.1021/es5002105.

Part-1
Scientific Reports
Volume 11: 11265
2021 年 5 月 28 日　公表済
DOI: 10.1038/s41598-021-90480-4

Part-2
Scientific Reports
Volume 12: 14738
2022 年 08 月 30 日　公表済
DOI: 10.1038/s41598-022-18900-7